University of Nevada, Reno

Hardrock Seismic Reflection Through Cover: Defining Controls on Mineralization via Reflection Attribute Analysis

A thesis submitted in partial fulfillment of the
Requirements for the degree of
Master of Science in Geology

by

Kyle Gray

Dr. John Louie, Thesis Advisor

December, 2013

University of Nevada, Reno
Statewide • Worldwide

THE GRADUATE SCHOOL

We recommend that the thesis prepared under our supervision by

KYLE T. GRAY

entitled

Hardrock Seismic Reflection Through Cover: Defining Controls On Mineralization Via Reflection Attribute Analysis

be accepted in partial fulfillment of the
requirements for the degree of

MASTER OF SCIENCE

John Louie, Ph.D., Advisor

Tommy Thompson, Ph.D., Committee Member

Sean Long, Ph.D., Committee Member

Jared Townsend, Committee Member

Alan Fuchs, Ph.D., Graduate School Representative

Marsha H. Read, Ph. D., Dean, Graduate School

December, 2013

Abstract

This study attempts to modify oil and gas industry seismic processing and interpretation techniques for use in Carlin-type deposit (CTD) gold exploration. Magmatic and deformation overprints on the Nevada carbonate platform-slope setting present challenges in seismic interpretation when compared to conventional seismic data, which is more commonly imaged in petroliferous basins with low levels of deformation. Barrick Gold Corporation provided 2D seismic reflection data for this case study, which assesses the viability of certain seismic practices when applied to hardrock seismic data collected in NE Nevada. Initial seismic interpretations of the pre-stack depth migrated (PSDM) sections located first-order structures and enhanced the geological model. This study uses derivatives of the PSDM, called seismic attributes, in an attempt to improve interpretability. Seismic attributes can reveal structural and stratigraphic features that are not apparent in the conventional PSDM amplitude data. Attribute analysis in this study leverages correlations made from a seismic response database of ~500 petrophysical drill core samples. These petrophysical measurements indicate that the ore zone exhibits a porosity, acoustic impedance, decarbonatization relationship that is distinguishable from unaltered rock. Down-hole geophysical data suggest an even larger contrast between altered and unaltered limestone. Given sufficient data quality, these observations make attribute analysis for detection of CTD alteration viable. An exhaustive calculation of attributes applied to one 2D reflection profile, which transects the Goldrush CTD resource, suggests that energy- and frequency-based attributes best

highlight the ore zone, which is expressed as a chaotic zone of reduced amplitude within one 2D profile. RMS amplitude and instantaneous amplitude identify broad zones of low amplitude whereas an average frequency attribute highlights possible high-frequency attenuation effects in the vicinity of the ore-zone. The sweetness and frequency washout attributes combine frequency and amplitude attributes to more effectively highlight the ore zone. However, the erratic response of sweetness and frequency washout suggest that they may be negatively affected by noise. One structural model is also presented, which used the instantaneous phase attribute to better visualize possible thrust faulting.

Acknowledgements

I would like to thank Barrick Gold Corporation for providing data and funding this research. My graduate degree was made possible with support from Paul Dobak, Barry Bourne, Jared Townsend and Brendan Howe. It has been my privilege to work with these industry experts at Barrick's Elko Exploration office. A special thanks to Jared Townsend and for his time as well as his open-minded approach to my research.

I would also like to thank my advisor, Dr. John Louie, for always supporting me (especially during my first two semesters at UNR). His guidance, knowledge and enthusiasm are unprecedented.

Dr. Amer Smailbegovic has also provided support throughout my career as a graduate student. I could not have made it without his guidance and financial support during the course of our consulting work. Furthermore, he has provided me with much of the industry experience required to succeed in the real world.

I also need to thank my committee members at UNR, Dr. Tommy Thompson, Dr. Sean Long and Dr. Alan Fuchs, for reviewing my work and providing necessary feedback. Also, a thanks to Dr. John Muntean is required for his advice and enthusiasm for my project.

Finally, I must thank my family and friends for dealing with my increased stress level and inflexible schedule in the past couple years.

Contents

ABSTRACT ..... **I**

ACKNOWLEDGEMENTS ..... **III**

CONTENTS ..... **IV**

LIST OF TABLES ..... **VII**

LIST OF FIGURES ..... **VIII**

INTRODUCTION **1**

1.1 MOTIVATION 4

1.2 GEOLOGY 5

1.2.1 Regional, Pre-Mineral Geology 5

1.2.2 Carlin Type Deposits 7

Structural Preparation 7

Stratigraphic Control 8

1.2.3 Local Geology 9

Stratigraphy 10

Alteration 11

1.3 ATTRIBUTE ANALYSIS 15

1.3.1 Simple Instantaneous Attributes 16

1.4 TIME DERIVED/GEOMETRIC ATTRIBUTES 17

1.4.1 Texture Attributes 17

1.4.2 Mathematically Combined Attributes 18

1.5 Petrophysics 19

1.5.1 Drill-Core Petrophysics 20

1.6 Challenges of Hardrock Seismic 23

1.6.1 Carbonate and Hard-rock Seismic Amplitude Versus Offset (AVO) 27

Background 27

Carbonates 28

1.7 Oil and Gas Industry Analogues 29

1.8 Seismic Data Used for This Study 33

1.8.1 Bandwidth and Amplitude Preservation 34

1.9 Complex Environment 35

1.10 Anisotropy 35

METHODS 36

2.1 Petrophysics 36

Data Collection 37

Data Preparation 38

Cross-plots and Impedance Contrasts 39

VSP data 39

2.2 Software 40

2.3 Drill hole Compilation 41

2.4 Attribute Calculation 41

2.5 Structural Interpretation 43

RESULTS 43

3.1 Petrophysics 43

3.2 Attributes 48

3.3 Structural Interpretation 51

3.4 VSP data 53

DISCUSSION 54

4.1 Petrophysics 55

4.2 Attribute Response 58

4.3 Structural Model 63

CONCLUSIONS 65

REFERENCES 68

List of Tables

Table 1 – Locations of previous hard-rock seismic studies within paleoplacer, layer mafic intrusion (LMI), sediment hosted, volcanogenic massive sulfide (VMS), Iron-oxide copper gold (IOCG) and intrusive complex settings. 26

Table 2- Acquisition parameters for Line 3..... 33

Table 3 – selected petrophysical properties subdivided by Wenban unit, brecciation and decarbonatization with standard deviation. Velocity is P-wave velocity..... 46

Table 4 – Calculated acoustic impedance contrasts for selected lithologic contacts based on drill-core petrophysics; calculations performed as first unit listed divided by second unit listed..... 47

Table 5- Averages from VSP hole with interpolated lithology logs from near-by core hole. 53

List of Figures

Figure 1 – Location of Carlin-type and sediment hosted mineralization occurrences and CTD trends within northeast Nevada overlain on state geology. Note the large spatial coverage of alluvial sedimentary rock residing in extensional basins and occurrences of large Au deposits within three trends. Au occurrences from the USGS Mineral Resource Data System (MRDS), State geology from Crafford (2007), RMT and craton boundary digitized from Muntean et al. (2011), Goldrush resource digitized from Barrick Annual Report, 2012. 3

Figure 2 – Location of the Goldrush/Red Hill resource adjacent to the Cortez Window and Cortez Hills Mine. Lower plate rock is in royal blue. The Northern Nevada Rift zone was digitized from a regional reduced to pole magnetic survey. Goldrush resource polygon digitized from Barrick Annual Report, 2012. 12

Figure 3 – The NNV Rift Zone, adjacent to the study area, is manifested as a large magnetic anomaly in reduced to pole magnetics..... 13

Figure 4 – Typical stratigraphy along Line 3 (formation descriptions from internal Barrick report; Cortez logging manual). 13

Figure 5 – Seismic section with superimposed drill hole data at a depth of 5500 to 4500 ft TVD. Au assay is shown to the left of the drill track and decarbonatization log is to right of drill track. 14

Figure 6 - Seismic section with superimposed drill hole data at a depth of 5500 to 4500 ft TVD. Au assay is shown to the left of the drill track and silicification log is to right of drill track. 14

Figure 7 - Seismic section with superimposed drill hole data at a depth of 5500 to 4500 ft TVD. Au assay is shown to the left of the drill track and clay log is to right of drill track. Note the absence of clays within the ore-zone. 15

Figure 8 – Brown's (2001) classification scheme for seismic attributes with the addition of texture attributes. Note that horizon attributes can only be applied to 3D datasets. 19

Figure 9 – Correlation between porosity and acoustic impedance in the Cortez Hills area. Included with permission from Smith (2010). Note that the author of this figure uses the term decalcification whereas the preferred term is decarbonatization... 22

Figure 10 – The left image shows synthetic seismic response and corresponding lithologies (Smith, 2010). The right image shows zero, 5-m-thick and 10-m-thick zones of decarbonatization (with greater vertical exaggeration; Smith, 2010). Note the zones of increased amplitude with the addition of a theoretical ore-body (arrows). 23

Figure 11– Seismic line 3 and drill holes in map view (above) and PSDM depth section (below) with approximate location of ore-zone outline by rectangle. The VSP hole is highlighted with a green drill track. Topography, in red, sampled from ASTER GDEM-V2. OpendTect and ArcGIS were used to plot the section and map, respectively. 34

Figure 12 – A portion of DW exhibiting anisotropic properties, which persist for 300 ft in this particular hole. 36

Figure 13 – Steering cube used to direct attribute calculations..... 42

Figure 14 – Acoustic impedance vs. porosity for all samples (i.e., Tertiary through Paleozoic), which is segregated on the basis of decarbonatization intensity. 45

Figure 15 – Acoustic impedance vs. porosity for the Wenban Formation. Note the two distinct trends: 1) decarbonatized denoted with red points and trend line, and 2) unaltered (blue trend). 47

Figure 16 – Spatial frequency (a), energy (b), sweetness (c), and frequency washout (d) attributes. There is no vertical exaggeration. 49

Figure 17- Instantaneous amplitude (a), GLCM entropy (b), similarity (c) and instantaneous phase (d) 50

Figure 18 – Two possible structural models with numbered drill holes. 52

Figure 19 – Crossplot of Vp and Vs down the VSP hole 54

Figure 20 – Porosity vs. theoretical acoustic impedance. Theoretical acoustic impedance was calculated with density values from decarbonatized core samples and a 3,705 m/s velocity from the VSP average 58

Figure 21 – Sweetness and frequency shadow attributes with modified color bars to highlight the ore-zone. Only the area of high seismic data-quality is shown (migration artifacts towards the margin of the dataset and basalts to the east are subset out of the view). There is no vertical exaggeration. 63

1 Introduction

This thesis is the result of collaboration with Barrick Gold Corporation, who provided high-resolution 2D seismic reflection data for detailed analyses. Four parallel, 2D seismic lines were designed to transect Barrick Gold's Goldrush resource, which is a concealed Carlin-type deposit (CTD) discovered in 2011. The resource is located in Horse Canyon, NV within the Battle Mountain-Eureka trend; the seismic lines, Goldrush resource and surrounding deposits are illustrated in Figure 1. This thesis focuses on seismic line number 3.

Reflection seismology has been used in the oil and gas industry for 85 years to define the soft-rock environment (Telford, 1990). More recently, the method has been successfully modified and employed for exploration of covered ore deposits associated with crystalline rock; for such cases, the term “hardrock” seismic has been adopted. Hardrock locations conducive to mineralization often exhibit complex geology due to multiple episodes of structural deformation and/or magmatism, which presents challenges to the seismic processor and interpreter alike. Regolith heterogeneity, ground relief and operating heavy machinery further complicate application of the seismic method.

This research has attempted to modify oil and gas industry surface seismic processing methods, such as attribute analysis and reservoir characterization, for use within the complex CTD environment. There are three goals: 1) seismically characterize

hydrothermal alteration features; 2) seismically characterize CTD formations, including those known to host gold; and 3) enhance our understanding of low-angle structural controls on mineralization. A catalogue of rock properties in the study area, established from petrophysical core sampling and a VSP borehole survey, allows for the observation of trends within rock units and alteration features. The broad goal of this research is to establish these petrophysical trends and highlight them in 2D surface seismic data using their seismic attributes.

Tanner (1991) defines seismic attributes as: “all the information obtained from seismic data, either by direct measurements or by logical experience-based reasoning”. In the oil and gas industry, seismic attribute analysis provides a means for prospect identification and reservoir characterization. The latter generally involves use of inversion or neural networks to relate multiple attributes to drill hole-properties in an attempt to predict petrophysical properties (e.g., porosity, fluid saturation, etc.; Hampson et al., 2001). This study involved an in-depth literature review of cutting-edge seismic methodologies to determine the techniques best suited to the CTD geologic setting. Seismic methodologies applied to mineral exploration largely focus on Precambrian volcanogenic massive sulfide (VMS), layered mafic intrusion (LMI) and mesothermal-type ore deposits. Accordingly, a strong emphasis is placed on oil and gas analogues (e.g., hydrothermal dolomite reservoirs).

During the course of this research, I have performed neural network (i.e., seismic facies classification, object detection and well-property prediction), geostatistical, and AVO

modeling, and both pre- and post-stack attribute analysis. However, this thesis focuses on gleaning geological and physical significance from single post-stack seismic attributes. After all, single attributes are the basis for the majority of advanced processing techniques and represent an efficient and effective approach for seismic interpretation.

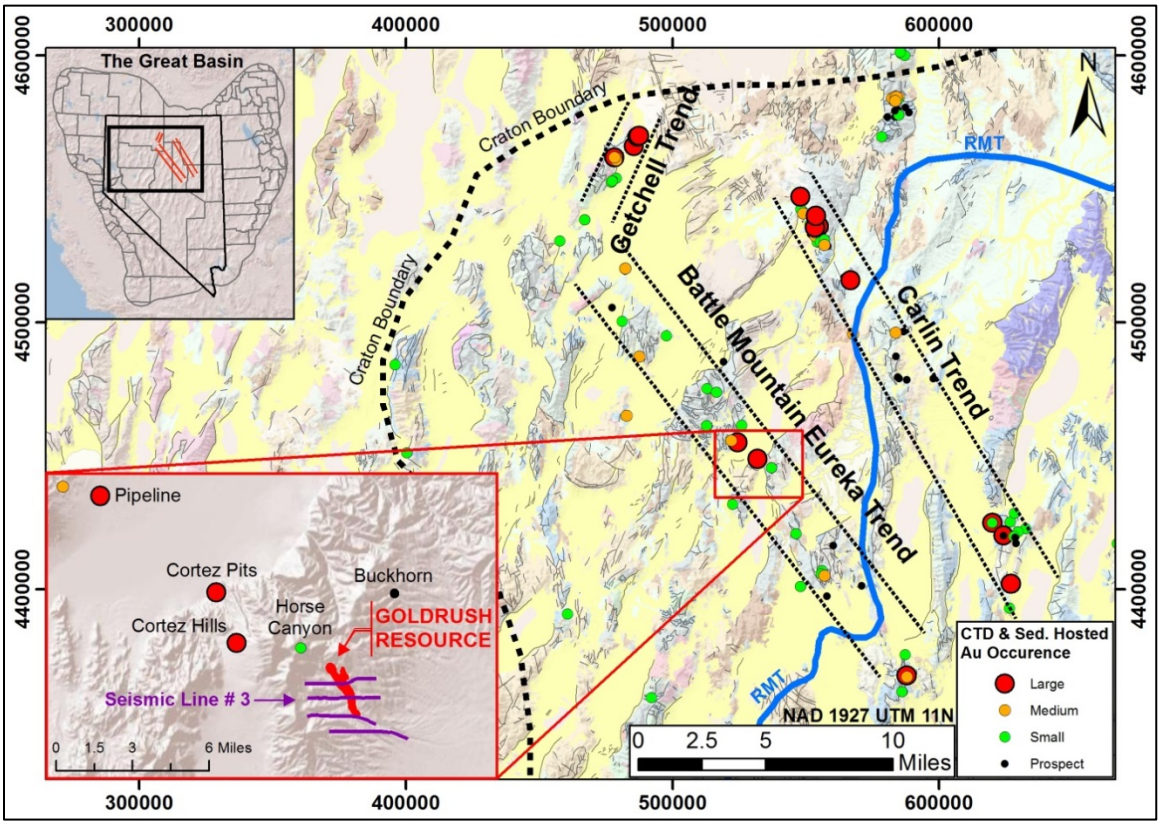

Figure 1 – Location of Carlin-type and sediment hosted mineralization occurrences and CTD trends within northeast Nevada overlain on state geology. Note the large spatial coverage of alluvial sedimentary rock residing in extensional basins and occurrences of large Au deposits within three trends. Au occurrences from the USGS Mineral Resource Data System (MRDS), State geology from Crafford (2007), Roberts Mtn. thrust (RMT) and craton boundary digitized from Muntean et al. (2011), Goldrush resource digitized from Barrick Annual Report, 2012.

1.1 Motivation

The Nevada state geologic map (Crafford, 2007) indicates that 49 percent of the state is covered by alluvial sediments that predominately fill north-south trending basins. This sediment can conceal CTDs of significant size (Muntean & Taufen, 2011). Since 1986, the majority of deposits have been discovered under shallow pediments through the projection of geochemical, geophysical, alteration, structural or lithologic features into the basin. More recently, exploration has been conducted within deeper portions of basins, outboard of the shallow pediment shelf. At greater depths, it becomes difficult to project geologic features from the bounding ranges. Furthermore, variability of physical rock properties across CTD inhibits the development of a systematic geophysical exploration approach for most traditional geophysical techniques such as the electromagnetic, induced-polarization, potential-field and radiometric methods (Townsend et al., 2010).

Subtle alteration features make direct geophysical detection of CTD challenging. This difficulty is further compounded by structural, hydrothermal, metamorphic and magmatic overprints of pre and post-mineral origins (Townsend et al., 2010). Traditional geophysical prospecting techniques used widely within the mining industry (i.e., magnetic, gravity and electrical methods) have limited sensitivity and resolving power at depth and are incapable of accurately defining deep structural and lithologic features important to mineralization (Urosevic & Kepic, 2008). High resolution reflection seismology offers a new and effective approach for CTD exploration under cover.

Seismic reflection surveys provide superior location precision because they are related to changes in the elastic properties of rock across a lithologic interface rather than traditional geophysical techniques, which show the total effects of all rocks within a subsurface region (Louie et al., 2011; 2012). Vertical variations between lithologies, typical of low angle decollement faulting and an evolving carbonate shelf-slope sequence, provide adequate acoustic impedance boundaries; such boundaries have facilitated seismic imaging of concealed thrust stacks and stratigraphy located beneath thick (i.e., greater than 1000 ft) alluvial fill. Accordingly, Barrick Gold Corporation has used reflection seismology for prospecting along the Cortez and Getchell trends.

1.2 Geology

1.2.1 Regional, Pre-Mineral Geology

The complex tectonic history of northeastern Nevada has produced a pre-mineral architecture conducive to the formation of CTD (Hofstra & Cline, 2000). Neoproterozoic rifting of North America produced basement penetrating rift faulting followed by the formation of a passive margin setting (Cline et al., 2005). A series of carbonate shelf-slope sequences, formed throughout the Paleozoic; these sequences were affected by the reactivation of basement penetrating rift faults that produced second-order basins within the passive margin setting (Muntean et al., 2007). Cook and Corboy (2004) identify several stages of platform margin architecture in northeastern Nevada: distally-steepened ramps with submarine fans (Late Cambrian-Early Ordovician) to low-angle homoclinal ramps (Late Ordovician), to rimmed platforms with slope debris aprons that

formed on low angle slopes (Silurian-Early Devonian) to rimmed margins with base-of-slope debris aprons that formed on steeper slopes (Early Devonian-Late Devonian).

During the Late Devonian and Early Mississippian, the Antler Orogeny and associated Roberts Mountain Thrust (RMT) drove eugeoclinal, deep-water siliciclastic and basaltic rocks 100-150 km eastward, placing them over the shelf-slope sequence (Cook & Corboy, 2004). The RMT separates lower plate carbonate rocks from upper plate eugeoclinal rocks. During the Antler Orogeny, the former continental slope and portions of the adjacent platform were warped downward to create a submerged foreland basin (Cook & Corboy, 2004). Siliciclastics were eroded from the Antler orogenic highlands and deposited eastward into the newly formed foreland basin (Cook & Corboy, 2004). After erosion of the highlands, shallow water Upper Mississippian and Lower Pennsylvanian carbonates were deposited over the basinal siliciclastics (Cook & Corboy, 2004).

Antler events were followed by the eastward emplacement of the Golconda allochthon during the Early Triassic Sonoma Orogeny. This was the ultimate orogenic event prior to the establishment of an east-dipping subduction zone along the western margin of North America. The subduction zone produced a magmatic arc and associated volcanic-plutonic complexes and lesser lamprophyre dikes during Mesozoic (Cline et al., 2005; DeCelles et al., 2004; Smith et al., 1993). Tertiary extension and magmatism overprint preceding events, forming a SE younging series of Eocene magmatic bodies followed by

Neogene Basin and Range faulting; these events are covered more thoroughly in the next section.

1.2.2 Carlin Type Deposits

CTD are sediment-hosted disseminated gold deposits of Eocene age (i.e., 36-42 Ma) characterized by decarbonatization of silty carbonates, which contain Au in solution or as submicron particles within disseminated pyrite or marcasite (Cline et al., 2005). Current Au production from CTD accounts for ~9 percent of world production and largely occurs along two N-NW trends, the Battle-Mountain Eureka and Carlin trends (Figure 1). Genetic models for ore formation vary but CTD are often coincident with or proximal to: 1) high angle NW-NE faulting possibly controlled by Neoproterozoic rifting structure; 2) Paleozoic thrusting and associated folds; 3) favorable carbonate host rocks capped by less permeable siliciclastics; and; 4) synsedimentary faulting (Cline et al., 2005; Muntean et al., 2007).

Structural Preparation

Structures often control the localization of ore within CTD. An intimate understanding of local structural architecture can aid in: 1) production of an accurate geological model, 2) characterization of mineralization, and 3) definition of drilling targets. There are three stages of faulting important to CTD, any of which may be linked to the aforementioned basement penetrating continental rift faults: 1) synsedimentary; 2) orogenic fault folding and; 3) Basin and Range faulting.

High-angle NE-NW-striking faults (e.g., range front normal faults) may act as conduits for deeply sourced fluid but low angle thrust faults may provide an important part of the plumbing system necessary for bedding parallel mineralization observed in some CTD (Nutt, 2005). These low-angle faults often propagate along contrasting rheological boundaries (e.g., formational contacts), which can act as detachment horizons to produce complex compressional faulting (e.g., duplex fault-fold culminations) (Leonardson, 2010). Furthermore, the eugeoclinal allochthon acts as a less permeable cap, which keeps mineralizing fluids in the reactive lower plate carbonates. These Paleozoic faults may have been reactivated during Tertiary extension, which would lead to increased permeability along the fault contact (Leonardson, 2010). This complex structural preparation, which can produce a network of permeable imbricate thrust faults, creates an environment susceptible to the formation of large CTD (Leonardson, 2010). In particular, axial crests of hanging-wall antiforms act as prime structural controls for mineralization in the Cortez area.

Stratigraphic Control

Exploration targets within the context of the Paleozoic continental margin include 3rd order lowstands (sea level regressions) that produce large-scale debris flows in the slope setting and subaerial exposure with associated karstification in the platformal setting (Cook & Corboy, 2004). These settings allow for increased porosity/permeability within a reactive carbonate mineralogy, which produces a good host horizon for mineralization (Cline et al., 2005). Synsedimentary faulting in the Paleozoic was caused by extensional

stress regimes or sedimentary loading (Cline et al., 2005). In either case, these faults can produce topographic highs that lead to debris-flow breccias and soft-sediment deformation, which further increases permeability within a stratigraphic horizon (Cline et al., 2005).

1.2.3 Local Geology

The Goldrush property is located within the Cortez District approximately 3 miles SE of the Cortez Hills mine. This district consists of geologic features common to many CTD: Cambrian to Devonian Lower Plate (below RMT), Cambrian to Devonian Upper plate (above RMT), Paleozoic overlap rocks, Mesozoic igneous activity, Eocene Intrusions, an Oligocene caldera and Miocene and Pliocene mafic extrusive rocks (see Figures 2 and 4). The district can be divided into two regions based on windows through the RMT, where lower plate carbonate rocks are exposed (Jackson et al., 2010). The two windows, Gold Acres to the west and Cortez to the east, are separated by Crescent Valley, a half-graben structure associated with Miocene (or younger) Basin and Range faulting (Jackson et al., 2010). Figure 2 shows the location of the Paleozoic windows and geology of the study area.

The Goldrush complex is located ~5 miles SE of the Cortez Window. The Au resource is hosted within a N-NW trending breccia mass thought to be located within a hanging-wall anticline, which was formed by east verging thrust faulting and possibly extension during the Paleozoic with possible reactivation during Neogene Basin and Range extension. The Paleozoic thrust fault is thought to be “soft-linked” to basement

penetrating rift faulting, which allowed for the influx of mineralizing fluids. The Paleozoic passive margin setting of this resource corresponds to the base-of-slope or slope apron model of Cook and Corboy (2004). The exact nature of the breccia body is unclear but it most likely represents a thick debris flow unit in the Devonian Wenban formation, which was overprinted by Paleozoic and Tertiary faulting.

The Northern Nevada Rift (NNR) is a prominent feature within the study area. The NNR is a mid-Miocene feature expressed by a NNW-striking magnetic anomaly and associated mafic dike swarms and volcanics (Figure 3). Geophysical modeling suggests the anomaly extends to mid-crustal depths and may represent preexisting crustal structure associated with continental rifting (Ponce & Glen, 2008).

Stratigraphy

Figure 4 represents typical stratigraphy found along Line 3. The RMT is completely eroded in the study area excluding allochthonous upper plate rock along Line 3; The Devonian Wenban Formation (DW) and Horse Canyon Formation (DHC) occupy the basin-fill/bedrock contact. The Paleozoic section within Line 3 is dominated by Dw, which is the Popovich Formation equivalent along the Carlin Trend. DHC is overthickened via thrusting locally to 200 meters in the Cortez District, although it is substantially less thick in the Goldrush area due to erosion. Dw is the primary gold host, which is substantially thicker than DHC due to repeated episodes of thrust faulting and the aforementioned erosion of DHC. Both units can be characterized as silty limestone,

although Dw is more proximal to the reef. Devonian Wenban Unit 5 (Dw5) is the most common host for brecciation, decarbonatization and mineralization.

Alteration

Figures 5 – 7 show a seismic section with superimposed drill hole logs of the three main types of alteration features present within the study area: decarbonatization, silicification and argillization. Alteration within the Dw along Line 3 is dominated by decarbonatization, which correlates well with Au content (Figure 5). Seven drill holes along Line 3 define a zone of strong decarbonatization that is 150-225 ft thick and extends 1300 ft laterally. Silicification is also present, although it is less frequent and more variable than decarbonatization (Figure 6). Clay is present within Tertiary volcanics but is nearly absent within the Dw, which is likely due to the scarcity of feldspar in limestone (Figure 7). It should be noted that clays resulting from argillization and structural (i.e. fault gouge) clays are both logged under the clay classification. Deep oxidation within the Dw is present, which is manifested by iron oxides within portions of the ore-zone. It is important to note that all alteration features are logged in a qualitative manner and each geologist may interpret weak, moderate and strong features differently.

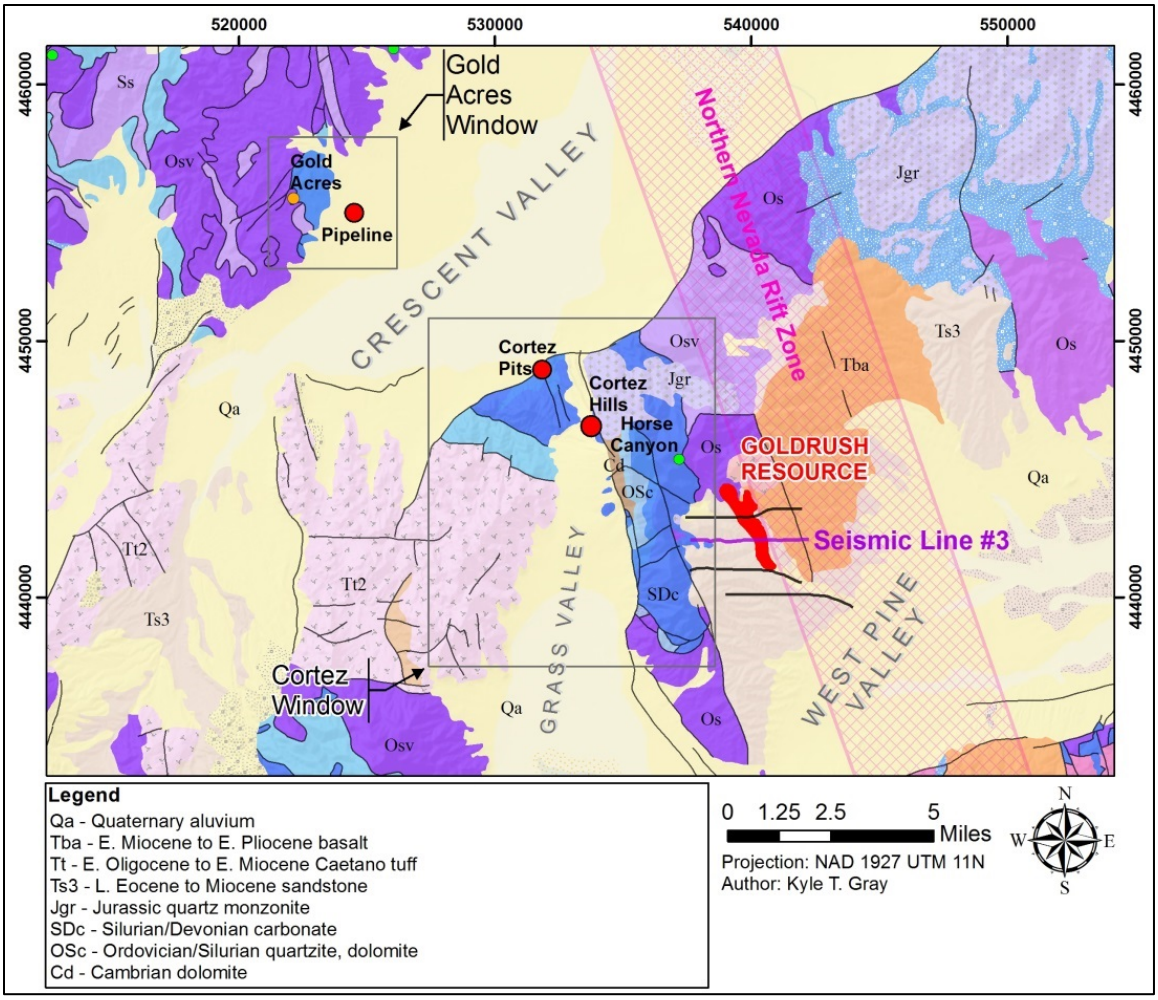

Figure 2 – Location of the Goldrush/Red Hill resource adjacent to the Cortez Window and Cortez Hills Mine. Lower plate rock is in royal blue. The Northern Nevada Rift zone was digitized from a regional reduced to pole magnetic survey. Goldrush resource polygon digitized from Barrick Annual Report, 2012.

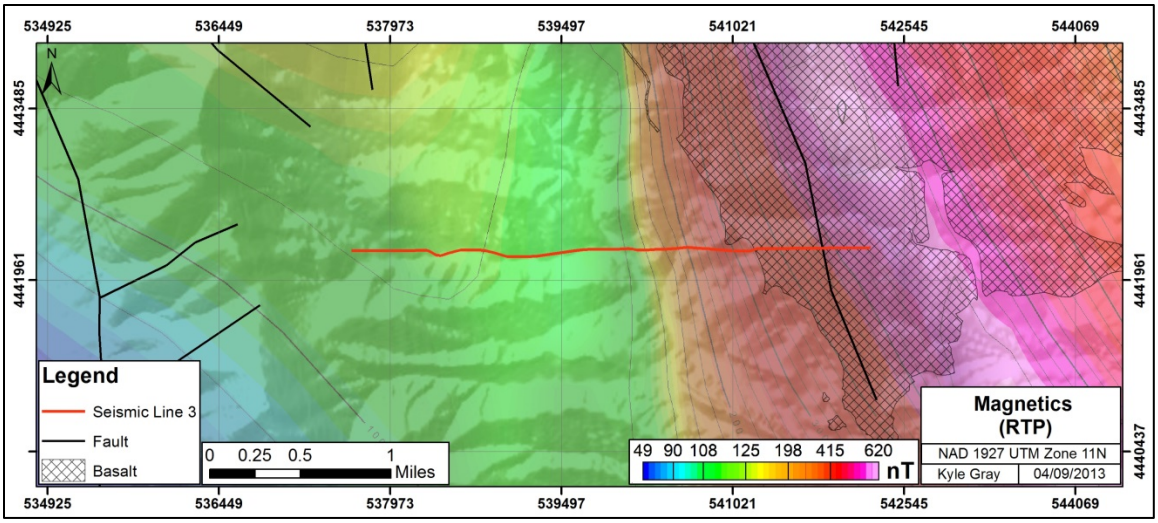

Figure 3 – The NNV Rift Zone, adjacent to the study area, is manifested as a large magnetic anomaly in reduced to pole magnetics (RTP). Note the basalt flow over Line 3.

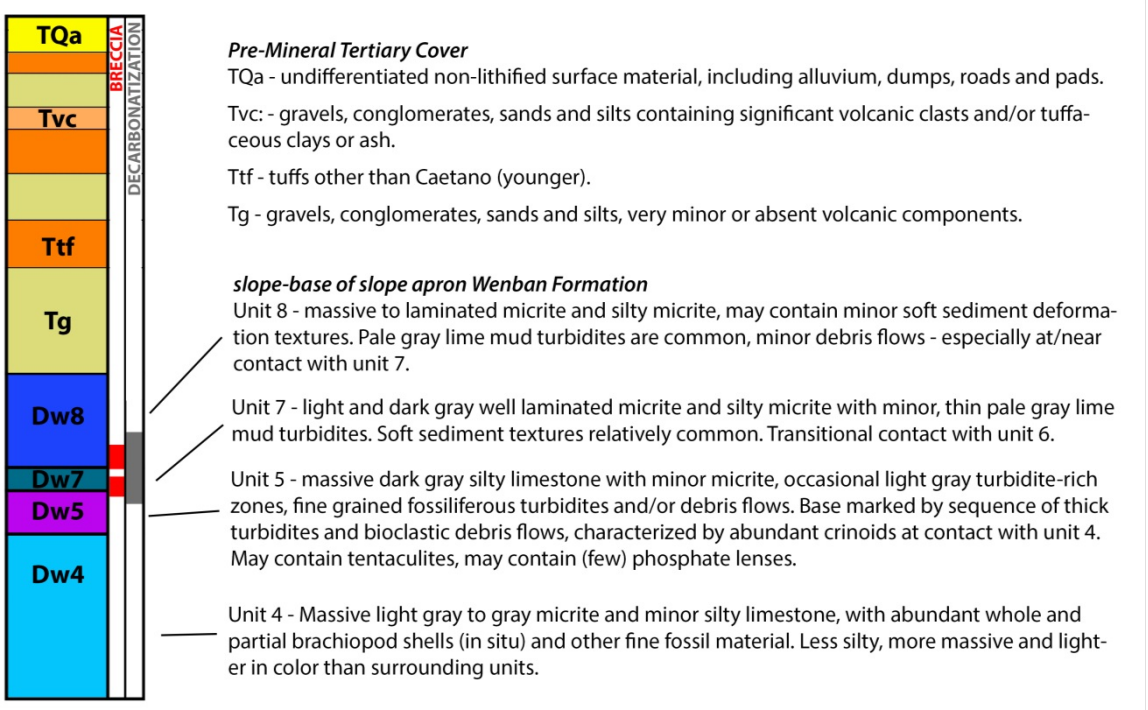

Figure 4 – Typical stratigraphy along Line 3 (formation descriptions from internal Barrick report; Cortez logging manual).

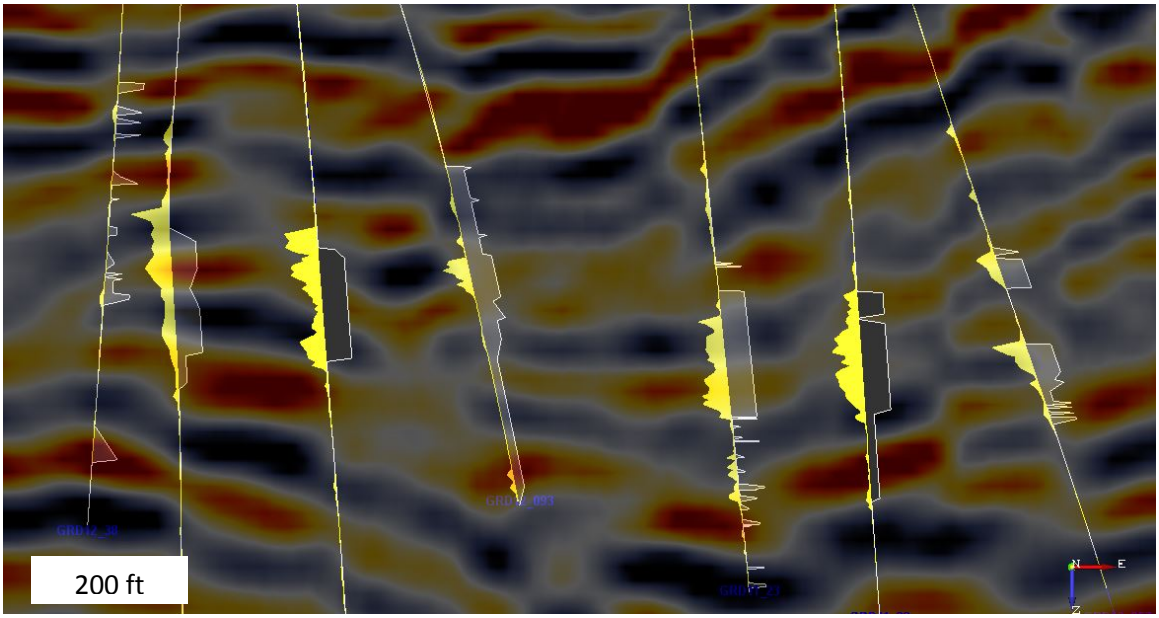

Figure 5 – Seismic section with superimposed drill hole data at a depth of 5500 to 4500 ft TVD. Au assay is shown to the left of the drill track and decarbonatization log is to right of drill track.

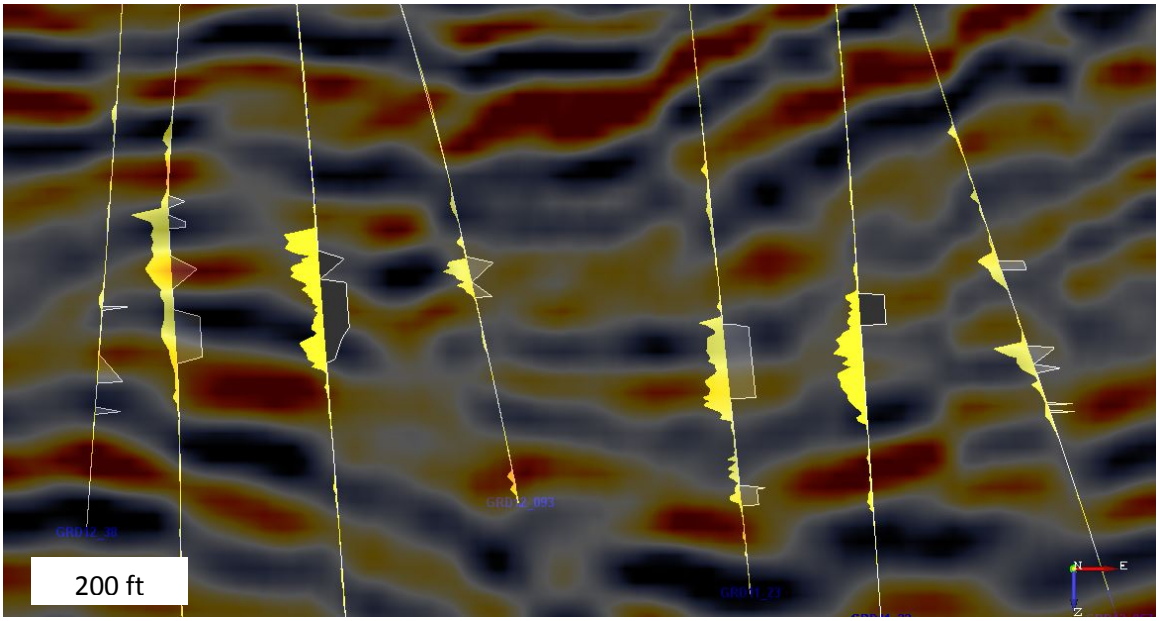

Figure 6 - Seismic section with superimposed drill hole data at a depth of 5500 to 4500 ft TVD. Au assay is shown to the left of the drill track and silicification log is to right of drill track.

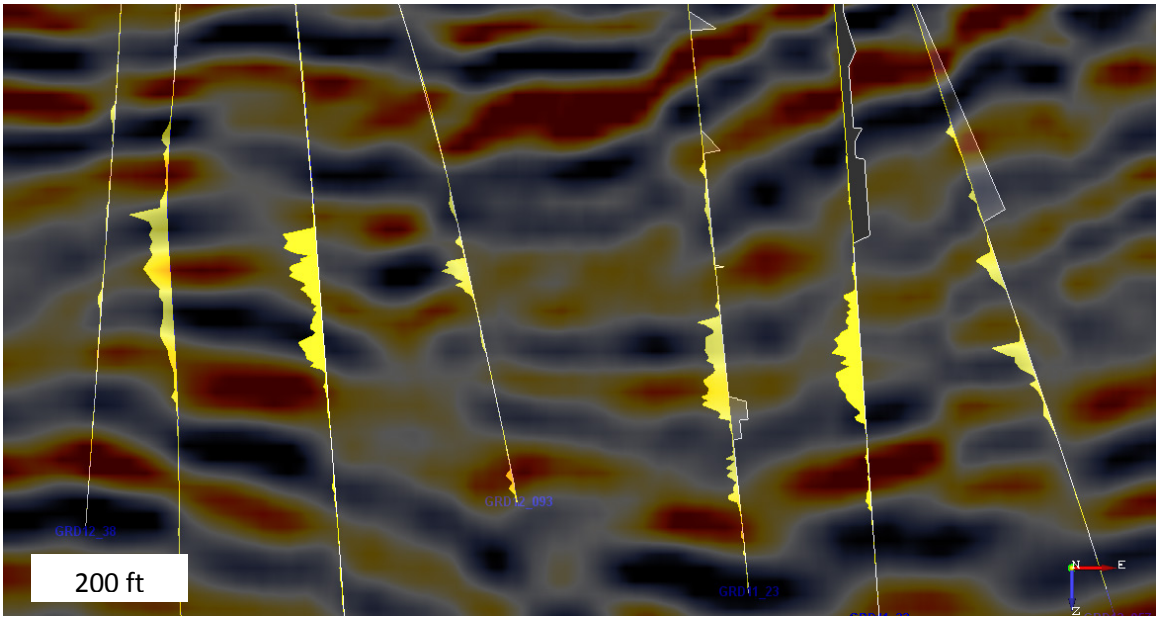

Figure 7 - Seismic section with superimposed drill hole data at a depth of 5500 to 4500 ft TVD. Au assay is shown to the left of the drill track and clay log is to right of drill track. Note the absence of clays within the ore-zone.

1.3 Attribute Analysis

Attribute analysis has gained popularity within the oil and gas industry in the past few decades (Chopra & Marfurt, 2005). Within the oil and gas industry these attributes allow for reservoir characterization, lithology prediction, and porosity forecasting in both siliciclastic and carbonate environments.

All seismic attributes take advantage of an infinite number of secondary quantities that can be derived from a primary seismic data cube (Liner, 2004). These quantities include geometric, kinematic, dynamic, or statistical features that can reveal geologic information not apparent in the amplitude data (Liner, 2004). The following sections will provide a brief overview of attribute classification schemes and information pertaining

to specific attributes in order to illustrate the breadth of options available to the seismic interpreter.

Attributes can be divided into four domains, which characterize the fundamental information contained within seismic data: time, amplitude, frequency, and attenuation (see Figure 8; Brown, 2001). Each of these domains has a specific application for interpretation; success in attribute analysis lies in the ability to select the most applicable attribute for the problem at hand (Brown, 2001). All attributes calculated in this thesis were applied to migrated and stacked data. The attributes used in this study can be divided into the following types:

1.3.1 Simple Instantaneous Attributes

Tanner et al. (1979) introduced the application of the Hilbert transform to seismic data, which allowed for instantaneous calculation of seismic amplitude, phase and frequency (i.e., one value for each parameter at each time sample of a seismic trace). Chopra and Marfurt (2007b) summarize the application of the three principal attributes:

1. Instantaneous envelope (reflection strength) is a measure of reflection strength and is sensitive to changes in acoustic impedance, which can highlight lithology and porosity changes.
2. Instantaneous phase can track reflector continuity and is useful for detection of unconformities, faults and lateral stratigraphic changes.

3. Instantaneous frequency is capable of highlighting abnormal attenuation and thin-bed tuning.

1.4 Time Derived/Geometric Attributes

Time derived attributes are most useful in extracting structural information from seismic data (Chopra & Marfurt, 2007a). Coherency, one of the most widely used attributes, measures lateral variations in waveform and/or amplitude within seismic data (i.e., trace-to-trace variations), which highlights discontinuity among reflectors (Brown, 2011). Dip and azimuth attributes examine reflector dip and azimuth based on a reference trace centered within a small analysis window. This method allows for the detection of subtle faults that have vertical throws of less than 10 ms in data with high signal-to-noise ratio (Chopra & Marfurt, 2007a). Curvature of dip and azimuth measures the curvature as the radius of a circle tangent to a curve; anticlines have positive curvature and synclines have negative curvature (Brown, 2011). This method helps remove effects of regional dip to emphasize small-scale fracturing. However, curvature is a second-derivative calculation of surfaces, which exacerbates noise.

1.4.1 Texture Attributes

Textural analysis via grey-level co-occurrence matrices (GLCMs) was implemented in the field of reflection seismology to aid in the process of manual seismic facies interpretation (West, 2002). The goal of these attributes is to mathematically describe pixel value distribution within a subset of the data (i.e., within the matrix). Accordingly, a transformation is applied to the data, which produces a GLCM of N by N dimensions,

where N is the number of gray levels used to quantify the data. Statistical operations are then applied to the GLCM, which describe the distribution of pixel values in different ways to produce various textural attributes. There are three groups of texture attributes (Chopra & Alexeev, 2005):

1. Contrast group (Contrast, Dissimilarity, Homogeneity): related to distance from the diagonal of the GLCM matrix along which neighboring values are equal. Attributes in this group: Contrast, Dissimilarity, and Homogeneity.
2. Measures related to orderliness: Angular Second Moment (ASM), Energy, and Entropy.
3. Group using descriptive statistics of the GLCM texture measures: GLCM Mean, GLCM Variance, GLCM Standard Deviation, and GLCM Correlation.

1.4.2 Mathematically Combined Attributes

Direct hydrocarbon indicators (DHI), such as the frequency washout and sweetness, combine multiple attributes via simple mathematical functions. Frequency washout is the energy of low pass filtered data divided by energy of high pass data. In frequency washout, the numerator gives energy in the low pass band and detects “shadows” whereas the denominator provides energy in the high-pass band and detects “attenuation”. High energy below the reservoir at lower frequencies is caused by attenuation from gas-filled sediments (Ebrom, 2004). Sweetness is defined as instantaneous frequency divided by instantaneous amplitude (Yushun et al., 2011).

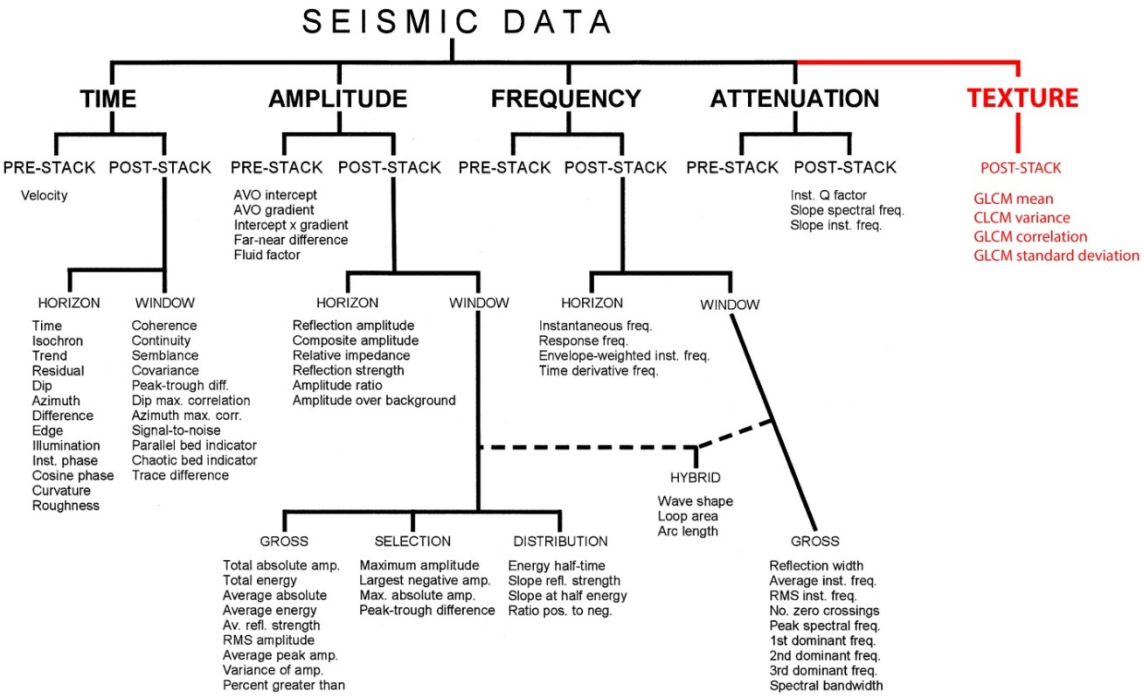

Figure 8 – Brown's (2001) classification scheme for seismic attributes with the addition of texture attributes. Note that horizon attributes can only be applied to 3D datasets.

1.5 Petrophysics

Direct petrophysical measurements, via lab samples or down-hole instruments, are a necessary component to bridge the gap between rock properties and surface seismic response. A seismic response database, consisting of drill hole logs and core sample measurements, is required to properly target mineralized rocks (Harrison & Urosevic, 2012). The elastic properties of mineralized and un-mineralized host rock must be fully understood in order to ascertain the feasibility of predicting lithological properties via surface seismic data (Harrison & Urosevic, 2012). The seismic response database helps one answer a very important question: Is the rock property variation sufficient to produce an anomaly in surface seismic data? The answer is often yes in the case of oil

and gas saturated siliciclastic reservoirs. However, the diversity of mineral deposit types in terms of host rock, alteration type and geologic setting produces a range of rock property variation that must be determined on a case-by-case basis within the mineral industry.

The formation of epigenetic ore-deposits requires increased porosity and permeability. Deposits formed in relatively recent geologic time (e.g., Cenozoic) often still exhibit zones of increased porosity, which greatly affects seismic parameters of the host rock.

An increase in porosity leads to decreased seismic parameters (i.e., bulk acoustic velocity and density). Scatter in the porosity-acoustic impedance relationship exists due to variations in pore shape, which is the most important factor influencing seismic properties (Wang, 2001). Rocks with flat, high aspect-ratio pores tend to exhibit lower seismic properties. Fracture porosity is formed by fracturing, which evolves to breccia porosity with increased movement along fracture planes. Compressional- and shear-wave velocities depend on the direction of wave propagation with regard to fracture orientation (i.e., anisotropic effects). However, if fractures are abundant and randomly oriented, the rock will behave isotropically (Wang, 2001); we presume that the Goldrush breccia would behave in this manner.

1.5.1 Drill-Core Petrophysics

Barrick has been conducting petrophysical core sampling in the vicinity of this prospect since 2009. Velocity, density and porosity measurements allow for characterization of

elastic properties in the selected samples. When combined with geologic logging records of alteration intensity and lithology, a robust dataset is produced, which can aid in bridging the gap between seismic response and rock properties. The majority of this data was collected by Barrick lab technicians. However, I personally performed analyses on ~50 samples in the vicinity of Dry Hills seismic Line 3.

It is important to note that samples measured in Barrick's petrophysics laboratory are biased towards competent or weakly altered rock. Strong decarbonatization results in dissolution and punky texture, which leaves a disintegrated and friable core sample. A solid, competent sample is required to properly measure velocity and density. Consequently, the most strongly altered rock is not sampled in the laboratory, which means that the petrophysics database is skewed towards higher density and velocity and lower porosity values relative to a truly representative population of rock samples in the Goldrush area. Furthermore, the petrophysical measurements will not include any fractures or other porosity larger than the sample diameter, which suggests that all core measurements set the upper bound for in-situ density and velocity.

Smith (2010) analyzed Barrick's seismic response database in 2009, which consisted of 92 core samples from the Cortez District (predominately Cortez Hills). Smith (2010) found that the Cortez District petrophysical measurements exhibited a strong inverse-linear relationship between apparent porosity and acoustic impedance as shown in Figure 9. The heavily decarbonatized zones exhibit increased porosity and a decrease in density and P-wave velocity. Smith (2010) also produced a zero offset synthetic

seismogram based on observations from the seismic response database. These results, shown in Figure 10 suggest the feasibility for acoustic impedance inversion and porosity interpolation between drill holes; Smith suggests that surface seismic data could be used as a means to identify zones of decarbonatization in the Cortez Hills region.

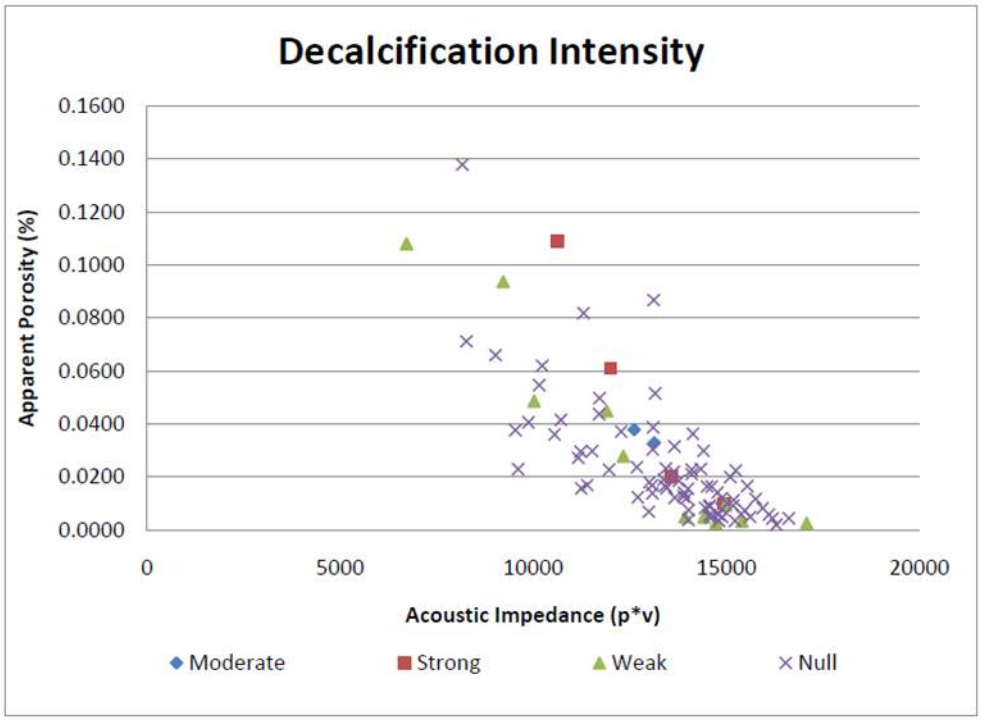

Figure 9 – Correlation between porosity and acoustic impedance Z in the Cortez Hills area. Included with permission from Smith (2010). Note that the author of this figure uses the term decalcification whereas the term used here is decarbonatization.

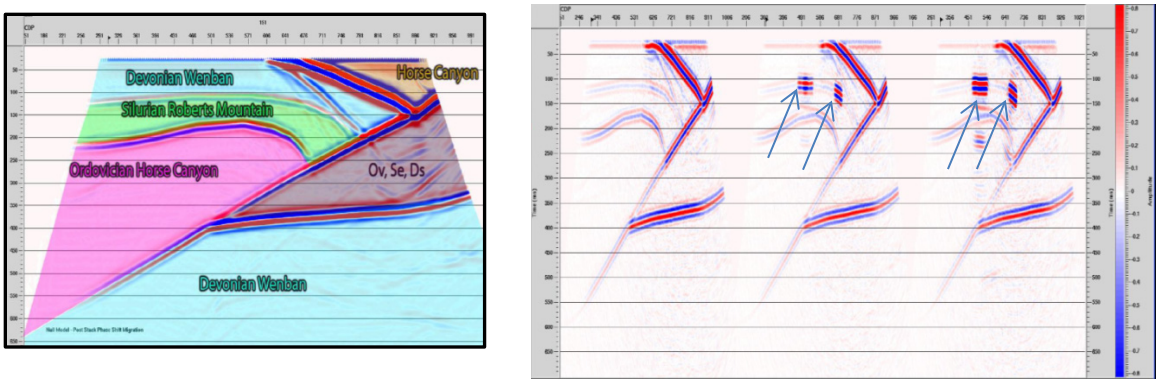

Figure 10 – The left image shows synthetic seismic response and corresponding lithologies (Smith, 2010). The right image shows zero, 5-m-thick and 10-m-thick zones of decarbonatization (with greater vertical exaggeration; Smith, 2010). Note the zones of increased amplitude with the addition of a theoretical ore-body (arrows).

1.6 Challenges of Hardrock Seismic

Table 1 provides an overview of hard-rock seismic studies performed for mineral exploration, most of which were located in Precambrian greenstone belts. These mafic, metamorphosed terranes contain seismically attenuated, high velocity rock that often destroys high frequencies, especially in the near-surface layer. A similar issue is encountered in the CTD setting, which relates to intercalated basalts and tuffs within tertiary alluvium and gravels. Accurate imaging and depth conversion are difficult and migrations suffer from much lower signal-to-noise levels when compared to the laterally continuous siliciclastic environment that is common to many petroliferous basins.

Seismic analysis of carbonates in the oil and gas industry is often based on a sequence stratigraphic framework. Seismic attribute studies predominantly aim to identify and highlight carbonate reefs, karst and channel features (Chopra and Marfurt, 2007b). These features are more difficult to image due to the heterogeneity of carbonate

stratigraphy and faster velocities relative to the siliciclastic environment. Furthermore, within the CTD setting, such features are significantly modified by orogenesis and no longer express their depositional morphologies at the seismic scale.

Higher density acquisition (i.e., close source/receiver spacing) in conjunction with detailed static corrections and velocity modeling are required to better sample and remove geological noise inherent to the hard-rock environment (Urosevic & Kepic, 2008). Down-hole seismic for velocity information becomes increasingly important in the hard-rock environment as well; such measurements are required to accurately locate the depth of reflectors, validate the presence of structures and properly implement seismic attribute analysis, AVO studies and inversion (Gibson et al., 2011).

Seismic exploration for ore-deposits often takes advantage of un-migrated stacks in search of diffractions, which are indicative of a possible massive sulfide body (i.e., high acoustic impedance boundaries such as a sulfide rich ore-zone or faulted gabbro host; Eaton et al., 2003). These features are observed as hyperbolic diffractions but require very large, localized acoustic impedance contrasts; such features are not associated with CTD seismic response. This method is most commonly performed for VMS-type exploration. Migrated data are often used for structural interpretation and location of geological features associated with mineralization. More advanced methods have looked at amplitude variations as direct indicators of ore. Forward modeling indicated bright spots at the Bell Allard ore deposit, which were subsequently confirmed in the surface seismic response of the deposit (Adams et al., 2003).

Most of the ore deposits imaged by seismic methods in the past have been located in the Precambrian environment; notable exceptions are the Tsumeb and Kombat deposits of Namibia discussed in Stevenson et al. (2003) and Boni et al. (2007). The Tsumeb Pb-Cu-Zn deposit is associated with a moderately folded and karsted dolomitic succession of the Otavi Group. The ore-body is located within and adjacent to an elliptical polymetallic pipe-like body that is approximately 150 m x 70 m. Synsedimentary fracturing linked to basement structures acted as a fluid conduit to produce the body. Mineralization occurs at the boundary between younger clastics and underlying dolomitic units. The Kombat Cu-Pb-Ag mine formed in a similar setting below a monoclinal flexure in carbonate rock. Physical property measurements indicate that the host rocks have average velocities between 3800 m/s (altered and fractured host rock) and 5130 m/s (unaltered host). The overlying clastic units have an average velocity of 3360 m/s. The seismic method was used to locate the contact between clastic and dolomitic units but paleo-karst features were not recognized. No seismic attributes are presented

Name, location	Setting	Age of ore genesis	Model	Author
Witwatersrand, South Africa	Igneous complex	Archean	Paleoplacer	(Eaton et al., 2003)
Bushveld, South Africa	Igneous complex	Archean	LMI	(Stevenson et al., 2003)
Namibia, South Africa (Tsumeb, Kombat)	Continental margin, paleo-karst	Tertiary	Sediment-hosted	(Stevenson et al., 2003)
Flin Flon, Quebec	Greenstone belt	Paleo-proterozoic	VMS	(White & Malinowski, 2012)
Mount Morgan, Australia	Fragmented pipe-like tonalite	Devonian	VMS	(Evans et al., 2003)
Bell Allard, Canada	Greenstone belt	Archean	VMS	(Evans et al., 2003)
Manitouwadge, Canada	Greenstone belt	Archean	VMS	(Evans et al., 2003)
St. Ives, Australia	Yilgarn Craton, mafic-ultramafic dome and shear zone.	Archean	Orogenic/ mesothermal	(Harrison & Urosevic, 2012)
Mt. Isa, Australia	Greenstone belt	Proterozoic	IOCG	(Evans et al., 2003)
Kristienberg, Sweden	Greenstone belt	Paleo-proterozoic	VMS	(Dehgannejad, 2012)
Pyhasalmi, Finland	Greenstone belt	Proterozoic	VMS	(Heinonen, 2012)
Half Mile Lake, Canada	Greenstone belt	Ordovician	Brunswick-type VMS	(Bellefleur et al., 2012)
Voisey's Bay, Canada	Greenstone belt	Paleo-proterozoic	Intrusive complex	(Duff et al., 2012)

Table 1 – Locations of previous hard-rock seismic studies within paleoplacer, layer mafic intrusion (LMI), sediment hosted, volcanogenic massive sulfide (VMS), Iron-oxide copper gold (IOCG) and intrusive complex settings.

1.6.1 Carbonate and Hard-rock Seismic Amplitude Versus Offset (AVO)

Background

Seismic sensors positioned at a range of distances, or offsets, from the energy source are a critical component of on-land reflection recording and imaging. A larger source-to-receiver distance generally produces a larger angle of incidence of the seismic wave on the reflector. Zoeppritz showed a century ago that seismic reflection coefficients for most reflective structures start at a few percent at normal incidence or zero incidence angle, and increase smoothly up to perhaps 30% at 50° angles, or offsets similar to the depth of the reflector.

In the early 1980's, Ostrander demonstrated that this general increase in reflection will change dramatically in the presence of gas; this phenomenon of offset-dependent reflectivity is known as amplitude variation with offset or AVO. The rock properties that cause AVO effects have been known for decades. However, improved acquisition, processing and interpretation techniques have only recently allowed us to derive and better understand the rock properties that produce AVO in real world data (Castagna et al., 1998). Knowledge is still limited in the realm of carbonates (Yongyi, 2008) and only one published study exists for AVO applied to mineral deposits (Harrison & Urosevic, 2012).

Wave energy is split into both P-waves and S-waves when a target is obliquely struck by an incident P-wave; the degree of mode-conversion is dependent on Poisson's ratio

(alternatively, the ratio of P-velocity over S-velocity, V_P/V_S), which is a measure of the material's lateral expansion under axial compression (Brown, 2011). Poisson's ratio is primarily a function of lithology and fluid content, although other factors such as clay content, cementation, pore shape and alignment, and porosity also play a role. The reflection response between the top of an oil and gas reservoir and its seal is of primary interest in most AVO studies, although effects are present wherever significant contrasts in Poisson's ratio exist (Brown, 2012).

Carbonates

Yongyi et al. (2008) performed a review on AVO effects in carbonate reservoirs in the Western Canadian Sedimentary Basin, which consists of dolomitized porous limestone reservoirs of Devonian age. The authors list several issues encountered when applying AVO in the carbonate environment: 1) a lack of carbonate rock property information, 2) differences between clastic AVO and carbonate AVO are not entirely understood, 3) procedures and calibration in seismic data processing need to be developed and improved for carbonates. They use dipole sonic logs in an attempt to overcome such issues and propose the "carbonate line", an alternative to the "mudrock line". Ultimately, they find that fluid content relates to offset dependent reflectivity within a porous carbonate reservoir encased by tight limestone.

Harrison and Urosevic (2012) performed the most advanced seismic study so far published in the mining community. They investigate the potential for AVO and seismic inversion for detection of gold mineralization in the St. Ives gold camp, Australia. Three

sonic logs were used to perform acoustic impedance inversion by several different methods: model-based, band-limited, colored and sparse-spike. AVO results indicate that far offset stacks (600-1200m) reveal amplitude anomalies coincident with gold mineralization, which suggests that variations in Poisson's ratio and shear wave velocity may contribute to the seismic signature of the ore body. Accordingly, elastic inversion was executed. A crossplot of elastic and acoustic impedance revealed zones of possible gold mineralization.

1.7 Oil and Gas Industry Analogues

Carbonate reservoirs account for over half of the world's petroleum reserves but have not been proportionately studied due to a concentration on clastic environments (e.g., Gulf of Mexico, Atlantic Ocean) in Western literature (Chopra & Marfurt, 2007b). The carbonate environment inherent to CTD shares geologic similarities with brecciated carbonate oil and gas reservoirs, which are often imaged via seismic reflection. These analogues are important to note so that similar processing techniques can be adopted for the identification of CTD alteration features in seismic data. This is one advantage of working in CTD over most hard-rock seismic mineral exploration programs, which are predominately located within the Archean Greenstone environment. Table 1 makes it clear that these previous hard-rock seismic exploration programs share few similarities with petroliferous basins.

Carbonate debris flow aprons can make excellent oil reservoirs (e.g., Tuxpan Platform, Mexico - several billion barrels; Loucks et al., 2011). This type of environment represents

the closest analogue to the Goldrush geologic model. The Poza Rica field, Mexico contains an apron that was deposited from an escarpment as much as 1,000 m high. A 20 m thick debris flow unit was formed, which produced discontinuous and hummocky reflections.

Hydrothermal dolomite reservoirs of the eastern United States and Canada represent another good analogue. Formation is thought to be related to one of two mechanisms: 1) karsting, or 2) dolomitization and silicification of the reservoir (Tedesco, 1994). Overall, these oil reservoirs bear a resemblance to a decarbonatized and brecciated CTD (with the exception of increased fluid content). Tedesco (1994) analyzed dolomite breccias of the Trenton-Black River formations, which extend from Central Tennessee to Southern Ontario. He notes that these reservoirs consistently exhibit six characteristics:

1) Breccia is located in a broad rubble zone within carbonate hosts replaced by secondary dolomite.
2) The breccia zone is encased by non-porous limestone or dolomite.
3) There is a close association with basement faults.
4) There is a structural sag above the reservoir, which is often accompanied by thickening of overlying units.
5) Thick reservoirs of 100 to 800 ft.
6) Narrow in width and elongated in length.

Tedesco (1994) then describes several seismic characteristics:

1) Amplitude dimming within the breccia.
2) Indications of basement faulting.
3) A sag at the top of the breccia zone.
4) Discrete zones of increased amplitude within the breccia, which represent rock property contrast between the breccia and isolated blocks of country rock.

Hart et al. (2004) note similar seismic signatures on hydrothermal dolomite but emphasize structural sag and amplitude dimming as the strongest seismic characteristics. They also introduce the concept of “low-velocity pull-down” from dolomitization (Hart et al., 2004).

Tang et al. (2011) successfully performed neural network classification of seismic attributes on the “complexly deformed” Wafra oil field. Reservoir rock consists of porous (occasionally vuggy) subtidal dolomite located within a zone of dextral shear. Facies prediction was guided by gamma ray, spontaneous potential, sonic, density, neutron, photoelectric and resistivity logs to define 8 distinct rock facies within the 3D seismic dataset. Unlike most neural network studies, Tang used multiple wire-line logs to train the network, rather than multiple attributes. This strategy resulted in facies classification with an accuracy of 75%. This study suggests the feasibility of well property prediction in the carbonate environment with sufficient wire-line log coverage. The average porosity of the reservoir is 15% and vuggy zones are common. However, the

complexity of overburden and deformation is less than that exhibited within the Goldrush complex.

Breccia gas chimneys also bear a resemblance to CTD environments, and have been extensively studied via neural network techniques in the oil and gas industry. Chimneys are observable on seismic sections as vertical zones of deteriorated data quality (Arnsten, Wensaas, Loseth, & Hermanrud, 2007). Increased seismic noise is associated with reduced acoustic velocities and gas presence in overburden rocks (Arnsten et al., 2007). Neural network techniques have been successful in mapping such chimneys (Meldhal et al., 2002; Ligtenberg, 2003, Heggland, 2004). Meldhal et al. (2002) produced an object detection neural network methodology to locate chimneys, which utilizes dip-steered and vertically oriented attributes such as energy and various types of trace-to-trace similarity.

Hydrocarbon bearing sands produce impedance changes that can produce bright spots and dim spots in seismic data. Brown (2012) stresses the importance of dim-spot detection for future reservoir discoveries. Impedance reduces when a reservoir becomes more porous, and reduces further when water-filled pores are replaced by hydrocarbons. If this hydrocarbon saturated reservoir is encased by higher impedance rock a bright spot is produced; if it is encased by a lower impedance rock a dim spot is produced. Dim spots are much more difficult to interpret than bright spots and are often overlooked. Brown (2012) also stresses the fact that there are many alternative reasons other than hydrocarbon effects that can significantly change amplitudes.

1.8 Seismic Data Used for This Study

The seismic reflection survey used as an input for attribute analysis is shown in Figure 11. This 2.8 mile survey was acquired by Tesla Exploration Ltd. Table 2 summarizes the acquisition parameters for the survey. The data were processed using a standard workflow that consisted of deconvolution, static corrections, migration velocity analysis and Kirchhoff pre-stack depth migration (PSDM). The data were processed in order to maintain true relative amplitudes, which is a requirement for detailed seismic attribute studies. Additionally, a walkaway VSP survey was conducted during surface seismic acquisition. The seismic data, which were acquired within the densely drilled Goldrush property, will act as a surface seismic study site in an attempt to extract relationships between seismic attributes and alteration features.

Sensor	Geo Space Corp.; GS-32CT; 70 %; 476 Ohm; 10 Hz High Spurious G
Filters	3 – 410 Hz
Sample rate	1 ms
Record length	3000 ms
Source	Explosive; single hole; 1 composites
SP interval	40 ft
Receiver array	6 geophones
Receiver interval	10 ft
Spread	484 groups per shot record
Max offset	2420 ft
Coverage	41-fold (max)

Table 2- Acquisition parameters for Line 3.

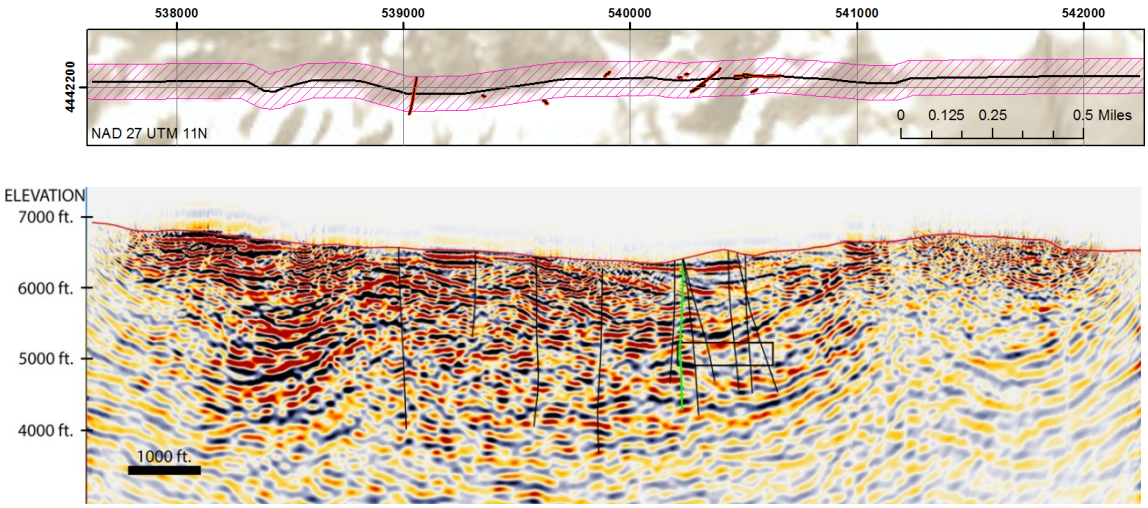

Figure 11– Seismic line 3 and drill holes in map view (above) and PSDM depth section (below) with approximate location of ore-zone outline by rectangle. The VSP hole is highlighted with a green drill track. Topography, in red, sampled from ASTER GDEM-V2. OpendTect and ArcGIS were used to plot the section and map, respectively.

1.8.1 Bandwidth and Amplitude Preservation

Increased bandwidth and amplitude preservation leads to attribute images with improved vertical and lateral resolution (Chopra & Marfurt, 2007b). Ideally, the vertical seismic profile (VSP) data collected on Line 3 should have been used to estimate seismic attenuation with depth, which could restore frequency components and account for amplitude attenuation within the surface seismic data (Chopra & Marfurt, 2007b). However, such procedures are untested in complex terrain. Furthermore, such a procedure could produce inaccurate attenuation estimates due to the VSP hole being located within an area of anomalous/intense alteration.

True-amplitude recovery is widely used in the application of amplitude variations with offset (AVO) studies but it is equally important when analyzing amplitude-based

attributes (e.g., energy, root-mean-squared amplitude, etc.). Most seismic imaging techniques strive to produce a geometrically accurate subsurface image with little regard for preservation of amplitude information (affected by geometrical spreading, transmission losses, improper focusing in areas of complex geology and AVO anomalies). The data processors aimed to preserve amplitudes but the complex geologic setting may have introduced errors due to smeared imaging.

1.9 Complex Environment

Data quality relates to three separate factors: 1) acquisition, 2) processing, and 3) complexity & heterogeneity of geology. Common image gathers (CIG) are one of the best indicators for the quality of depth imaging (MacKay, 2011); in the case of our data, the events in the pre-stack domain are fairly flat given the circumstances of complex geology and 2D acquisition. However, under basalt, to the east, pre-stack events are very chaotic and noisy. Fortunately, this area is outside of the ore zone and should therefore not adversely affect attribute analysis on Line 3.

1.10 Anisotropy

The seismically derived velocities along Line 3 are expected to have a horizontal component of uncertainty due to the effects of anisotropy (Tsvankin & Thomsen, 1994). Anisotropic effects were not directly measured in the laboratory via triaxial core tests but Figure 12 illustrates an interval of Dw7 with parallel fracturing along bedding planes. Analysis of drill core photos suggests that Dw exhibits transverse anisotropic properties in unaltered intervals, which generally range from 100-300 ft in thickness throughout

the majority of Line 3. The presence of anisotropy can negatively affect migration velocity methods such as semblance analysis.

Figure 12 – A portion of Dw exhibiting anisotropic properties, which persist for 300 ft in this particular hole.

2 Methods

2.1 Petrophysics

Both Yonyi (2008) and Harison & Urosevic (2012) stress the importance of cataloging rock-property information to better understand the significance of lesser-known AVO effects in carbonate and hard-rock settings.

A total of 566 core samples in 39 different drill holes were collected in the Goldrush area at 50-100 ft sampling intervals from 2009-2013; these samples represent Quaternary alluvium, Tertiary gravels and volcanics, Devonian Horse Canyon Formation and Devonian Wenban Formation (Dw4, Dw5, Dw7 and Dw8). However, reverse-circulation (RC) drilling is used in the majority of the Tertiary section so petrophysical sampling is limited for alluvium, gravels and volcanics. VSP P-wave velocity and S-wave

velocity were also used to supplement the drill-core data and have the valuable benefit of sampling the Tertiary section. The ultimate use of the petrophysical drill hole data is three-fold: 1) produce cross-plots to isolate alteration features based on petrophysical characteristics; 2) determine acoustic impedance contrast between alteration features and Dw units and 3) create pseudo-logs for neural network training and cross-validation.

Data Collection

The petrophysical measurements are collected from half core samples of NQ diameter. The ends of the core are cut orthogonally to a final length of four to eight inches; cutting also produces smooth surfaces for instrument contact. An ultrasonic velocity meter is used to calculate P-wave velocity. 54 KHz transducers are placed on each end of the cut core and the sample length is entered into the meter. The transducers emit an electrical pulse that is converted to a pulse of ultrasonic vibration that travels through the core. The signal wavelength is about 100 mm, depending on the velocity of the rock. The wave is converted back into an electrical pulse once it reaches the other transducer so that transit time can be recorded and used for the calculation of P-wave velocity.

Bulk density calculations, which are based on Archimedes method, require three measurements: dry mass, saturated mass, and submerged mass. The dry weight of the sample is recorded and the sample is subsequently soaked in water overnight to replicate in-situ saturation. Saturated weight is then recorded followed by submerged weight, in which the sample is submerged in water and weighed. Density can now be

calculated via a series of equations beginning with Archimedes method to determine bulk volume. Dry bulk density is then determined by dividing dry mass by bulk volume.

Data Preparation

Since the ore-body is located entirely within the Devonian Wenban Formation (Dw), a Dw subset of the petrophysics data was created to isolate specific alteration features and units within this formation. As a starting point, a Dw unaltered database was produced, which consisted of 171 core samples that were logged with no brecciation (RBX or SBX), decarbonatization, argillization (clay content), or silicification. The Dw unaltered database was further divided into specific Wenban units: Dw8 unaltered, Dw7 unaltered, Dw5 unaltered and Dw4 unaltered. Dw Unit 5 (Dw5) contains the majority of alteration; accordingly, we are most concerned with the rock property contrast between altered rock and unaltered Dw Unit 5. Decarbonatization and brecciation represent the two alteration features known to best correlate with the ore-zone. Accordingly, the database was further separated into Dw brecciated (Dw RBX) as well as three classes of Dw decarbonatization: weak, moderate and strong. Finally, a generalized Dw decarbonatized database was produced, which consisted of all Dw samples marked as strongly or moderately decarbonatized.

A compensation factor of 0.96 was applied to the ultrasonic drill core measurements in order to account for the high frequency source relative to field seismic acquisition. This allows for proper comparison of VSP velocities against ultrasonic lab velocities. This factor was derived by Mustagh Resources Ltd., a seismic contractor employed by

Barrick, who utilized velocity relationships found in Sams et al. (1997). Cross-plots can now be prepared with the intent of isolating alteration on the basis of petrophysics.

Cross-plots and Impedance Contrasts

Cross-plots were produced based on conclusions made by Smith (2010), which focus on relationships between porosity, acoustic impedance and decarbonatization intensity. Separation of trends between unaltered and altered (i.e., decarbonatized and/or brecciated) are of particular interest.

Acoustic impedance contrasts were calculated for the following key lithologic and alteration boundaries pairs: Dw8 & Dw7, Dw7 & Dw5, Dw5 & Dw breccia, Dw5 & Dw decarbonatized. Calculations are based on zero-offset reflectivity.

VSP data

Unfortunately, the VSP data were collected in an RC hole, which makes lithologic logging more difficult; Dw4 was the only unit of the Wenban that could be differentiated within the Dw Formation. To overcome this issue, a nearby core hole (GRD11-38) was used to interpolate Dw8, Dw7 and Dw5 laterally to the VSP hole. The core hole is no more than 125 ft away from the VSP hole. This allowed for calculation of average P-velocity and S-velocity for specific units within the Wenban formation. Gardner's equation was used to approximate density in the VSP hole (Gardner et al., 1974).

Gardner's empirical equation was used to calculate density from the VSP P-wave velocity (Equation 1). Miller (1994) analyzed a series of Paleozoic carbonates from Alberta to test the validity of Gardner's equation when applied to limestone and dolomite; the carbonates studied have similar rock-properties to those found in the Goldrush area (i.e., high velocity, ~6000 m/s; relatively low porosity, 5-15% in porous zones and Paleozoic in age). Results, when compared to measured well-log densities, indicate that Gardner densities were accurate except when applied to zones of increased porosity, where density was slightly overestimated.

$$\rho = 0.23 V_p^{0.25} \text{ (ft/s)}$$

Equation 1 – Gardner's equation (Gardner et al., 1974)

2.2 Software

Two software packages were employed: dGB Earth Sciences OpendTect and Hampson-Russel HRS9. OpendTect was the primary software used to calculate attributes whereas HRS9 was used only used for visualization of drill hole data for this thesis.

OpendTect is available through a GNU open-source licensing agreement and is capable of: 2D, 3D and drill hole visualization, horizon tracking, calculation of dozens of attributes and 2D cross plotting of attribute vs. attribute or attribute vs. drill hole data. Optionally, the software can be extended through closed-source plugins; the dip-steering plugin was required for this study and provided by dGB Earth Sciences under an academic licensing agreement between UNR and dGB Earth Sciences.

2.3 Drill hole Compilation

Drill holes used in this study were all located within ~200 ft of Line 3 in order to diminish out-of-plane interpretations; a total of 13 holes met this criteria. Drill hole survey information was adjusted to match the seismic reference datum (SRD) and drill tracks were imported into the seismic software as ASCII files. Alteration features and rock types, logged from RC chips and core by Barrick geologists, were then imported to display along the deviated drill tracks. Silicification, argillization and decarbonatization are logged as null, weak, moderate or strong; these logs were assigned number values of 0, 1, 2 and 3, respectively, and subsequently imported into the software. Marker logs were produced for lithology and brecciation and imported as well; these markers read top down. Finally, Au assay values were imported (only relative abundance is shown to maintain confidentiality).

2.4 Attribute Calculation

Figure 8 illustrates many of the attributes that were calculated and examined over the ore zone in order to determine if any single attribute exhibited a unique response to mineralization features (with the exception of horizon-based attributes, which require 3D data). For the sake of brevity, only the most useful attributes are discussed and presented within this thesis.

In addition to the PSDM provided by the contractor, a smoothed version of the seismic data was also used as an input for attribute calculation. Smoothing was accomplished via a lateral medial filter with a 6-trace (60-ft) step-out. The resultant smoothed data

were then subtracted from the original PSDM as a test to ensure that only incoherent noise was removed. Ultimately, the smoothed data were only used as an input for instantaneous phase and similarity. Attributes used to define the ore zone (i.e., those that highlight amplitude and frequency changes) were calculated from the original PSDM since it was believed that incoherent reflectors may be present within the brecciated ore-zone.

Chopra and Marfurt (2007a) stress the importance of calculating attributes along reflector dip and azimuth (line dip in the case of 2D data). The OpendTect developers also recognized the importance of reflector dip and azimuth for attribute analysis and therefore developed a suite of methods to execute dip-steered attribute calculation. The precise FFT method was used for Line 3 due to its ability to handle increased noise; this method takes 10 times longer than other algorithms and is recommended for sections with lower S/N. Similarity and texture attributes were directed along line dip using the background steering cube.

Figure 13 shows the steering cube used to direct attributes along reflector dip.

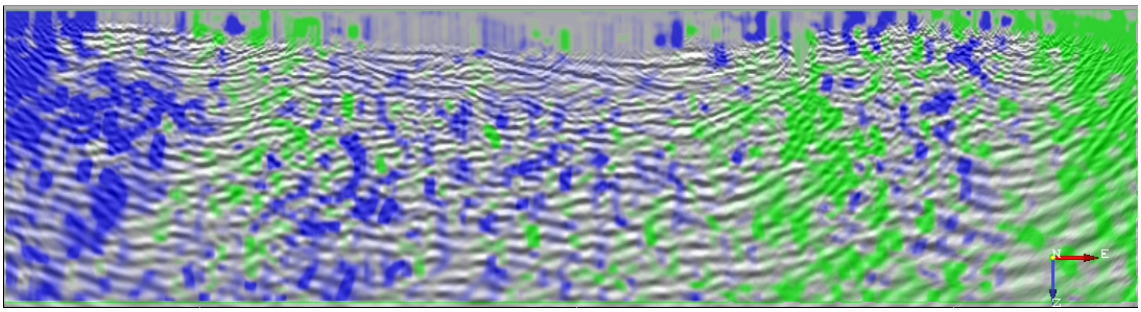

Figure 13 – Steering cube used to direct attribute calculations. Blue colors indicate east dipping reflectors and green colors indicate west dipping reflectors

2.5 Structural Interpretation

Structural interpretation of Line 3 is a secondary goal of this study. Two possible models are presented in the next section, and are based on seismic and drill hole lithologic log interpretation. Instantaneous phase, the PSDM, and bandpass filtered versions of the PSDM were used to identify reflector discontinuity in pursuit of a refined structural model for Line 3. Instantaneous phase has been used for structural interpretation for over a decade (Chopra and Marfurt, 2007b). Only drill holes within 200 ft (and mostly within 100 ft) of Line 3 were used to correlate with specific reflectors in an attempt to eliminate out-of-plane lithologic information. However, all four seismic lines and numerous drillholes were considered in producing a viable model for Line 3.

The following general rules of thrust belts were followed during interpretation (e.g., Boyer & Elliott, 1982): 1) thrust faults typically cut up-section in the direction of transport; 2) thrusts either repeat no stratigraphic section (i.e. occupy a decollement horizon), or place older rocks on younger rocks (duplicate stratigraphic section), but typically do not omit stratigraphic section; and 3) thrust faults typically develop parallel or at relatively low cutoff-angles (≤ ~20-to-30°) to bedding.

3 Results

3.1 Petrophysics

Figure 16 illustrates that the complete petrophysics database exhibits an inverse-linear correlation between porosity and acoustic impedance. Two trends became apparent

within this cross-plot, which separate the dataset based on intensity of decarbonatization; moderate and strongly decarbonatized samples exhibited lower acoustic impedances and higher porosity when compared to weakly and null decarbonatized samples. A stronger separation of trends became apparent in the Dw subset.

Table 3 presents average porosity, density and acoustic impedance for Dw units, Dw breccia and Dw decarbonatized. Dw unaltered (i.e., no DECAL, no ARGIL/CLAY and no SILIC) exhibited little to no correlation with porosity and acoustic impedance whereas the Dw decarbonatized population exhibited an inverse linear trend (see Figure 15). The calculated acoustic impedance contrasts for Dw units, brecciation and decarbonatization are presented in Table 4. Acoustic impedance is quite similar for all subsets and indicates that only the Dw5/Dw7 contact would exhibit a strong reflection.

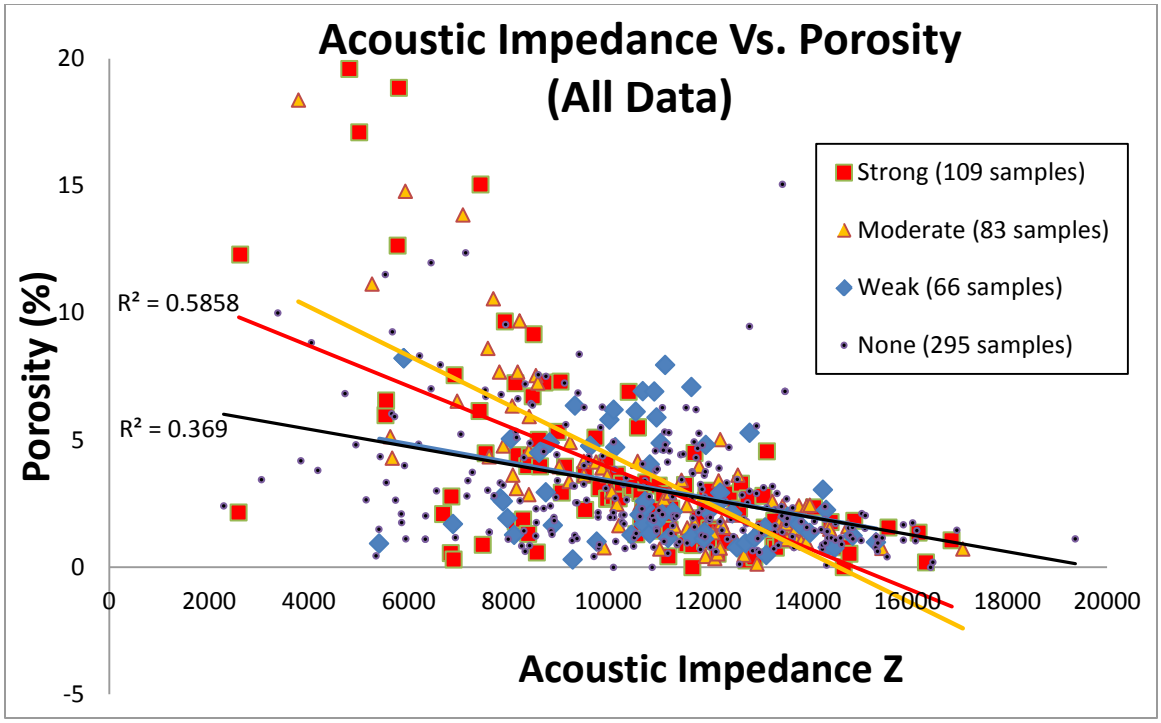

Figure 14 – Acoustic impedance vs. porosity for all samples (i.e., Tertiary through Paleozoic), which is segregated on the basis of decarbonatization intensity.

Unit	# of samples	density (g/cc)	std density (g/cc)	Porosity (%)	std porosity (%)	velocity (m/s)*	std velocity (m/s)	Acoustic Imped. Z
Dw8 (Unaltered)	27	2.56	0.17	3.45	2.94	3805	1091	10132
Dw7 (Unaltered)	15	2.61	0.07	3.62	2.21	3533	938	9620
Dw5 (Unaltered)	61	2.61	0.15	2.92	2.42	4162	1015	11305
Dw4 (Unaltered)	70	2.64	0.23	2.55	2.12	4027	882	11090
Dw-RBX	41	2.63	0.12	3.34	3.25	3901	664	10949
Strong DECAL	171	2.59	0.15	3.42	3.20	3730	822	10789
Assumed Strong DECAL	N/A	2.30	N/A	?	N/A	3600	N/A	8280

*P-wave ultrasonic drillcore velocities adjusted to seismic velocities via 0.96 compensation factor

Table 3 – selected petrophysical properties subdivided by Wenban unit, brecciation and decarbonatization with standard deviation. Velocity is P-wave velocity.

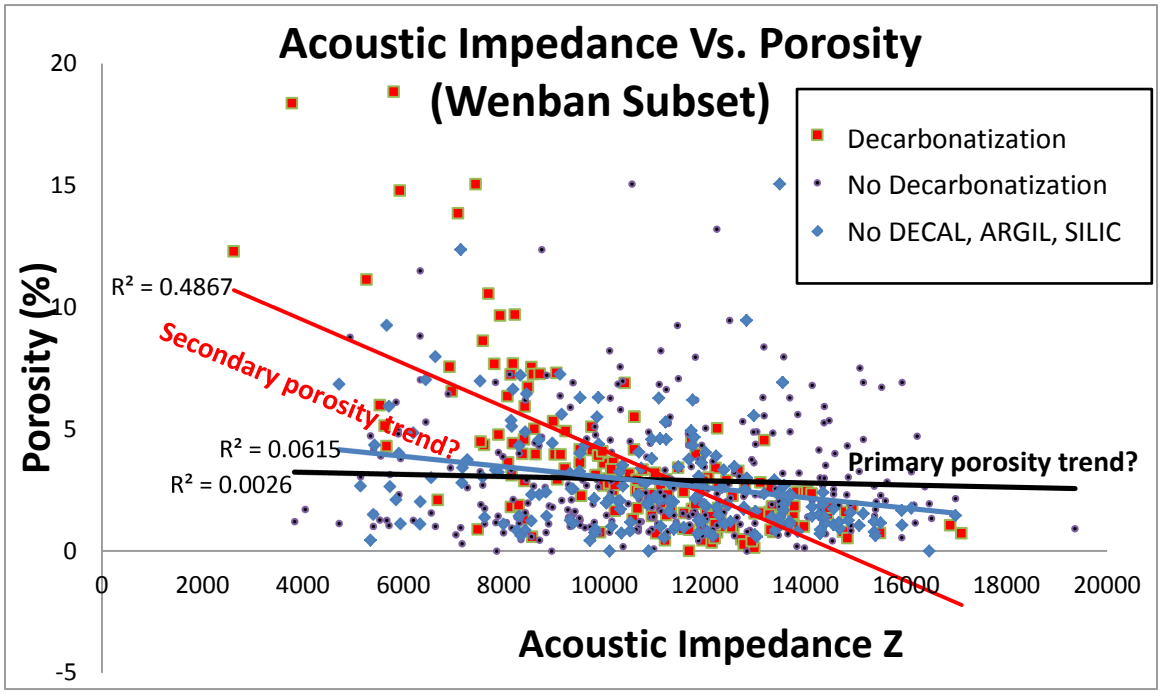

Figure 15 – Acoustic impedance vs. porosity for the Wenban Formation. Note the two distinct trends: 1) decarbonatized denoted with red points and trend line, and 2) unaltered (blue trend).

Contact	Z contrast
Dw8 & 7	0.026
Dw7 & 5	-0.081
Dw5 & 4	0.010
Dw5 & Dw-RBX	0.003
Dw5 & Dw-Strong DECAL	0.014
Dw5 & assumed Strong DECAL	0.154

Table 4 – Calculated proportional acoustic impedance contrasts for selected lithologic contacts on the basis of drill-core petrophysics; calculations performed as first unit listed divided by second unit listed.

3.2 Attributes

Figure 16 and Figure 17 display a series of attributes that best characterize the ore-zone and assist with structural interpretation. All Figures include the ore-zone as a box as well as the Dw horizon pick (where interpretable). Single attributes revealed low values for frequency, instantaneous amplitude, energy, GLCM entropy, and high values for sweetness and frequency washout. However, a degree of variation is present for every attribute within the ore-zone.

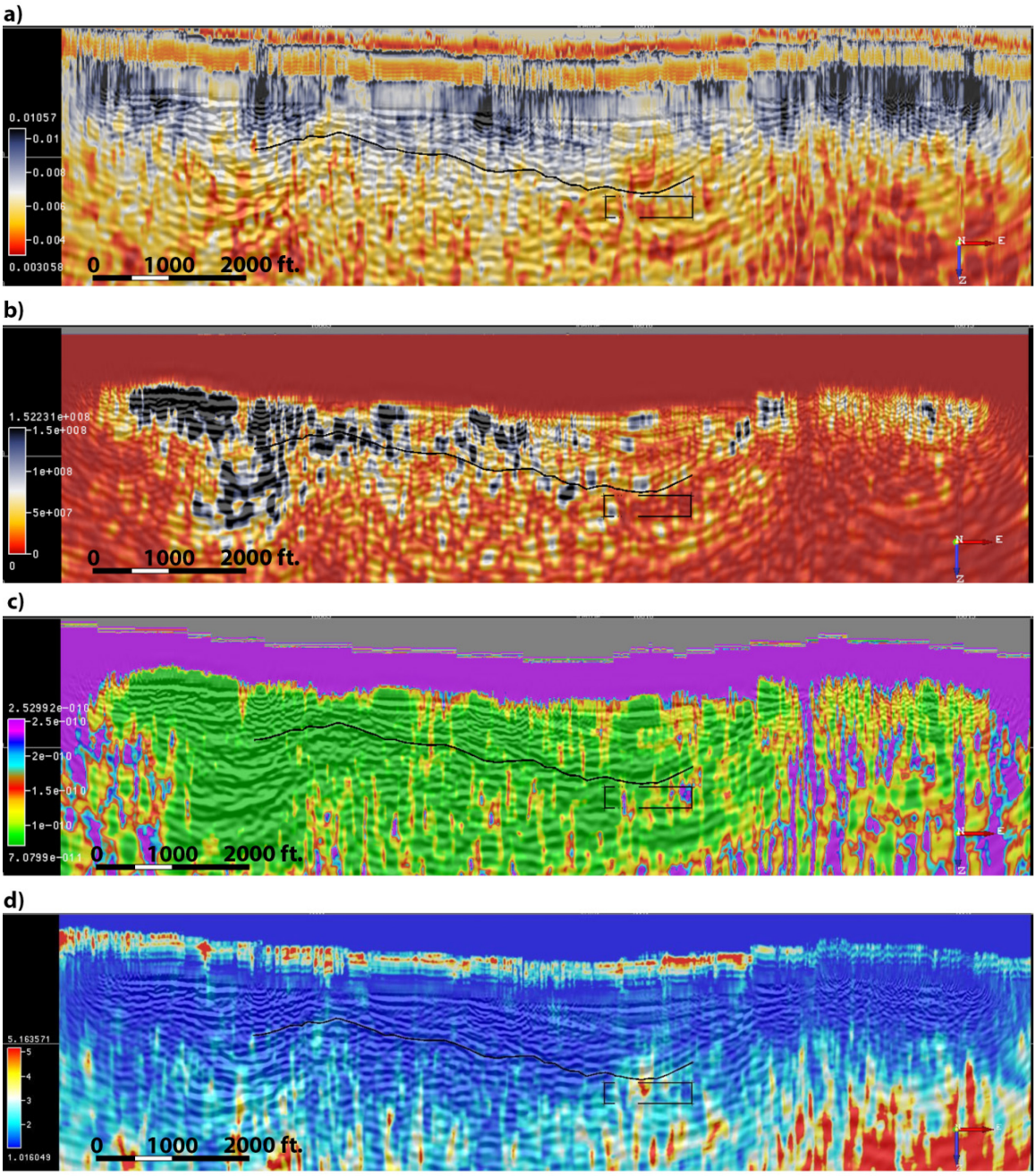

Figure 16 – Spatial frequency (a), energy (b), sweetness (c), and frequency washout (d) attributes. Thin black lines mark the bottom of the Tertiary section, and a black box marks the ore zone. There is no vertical exaggeration.

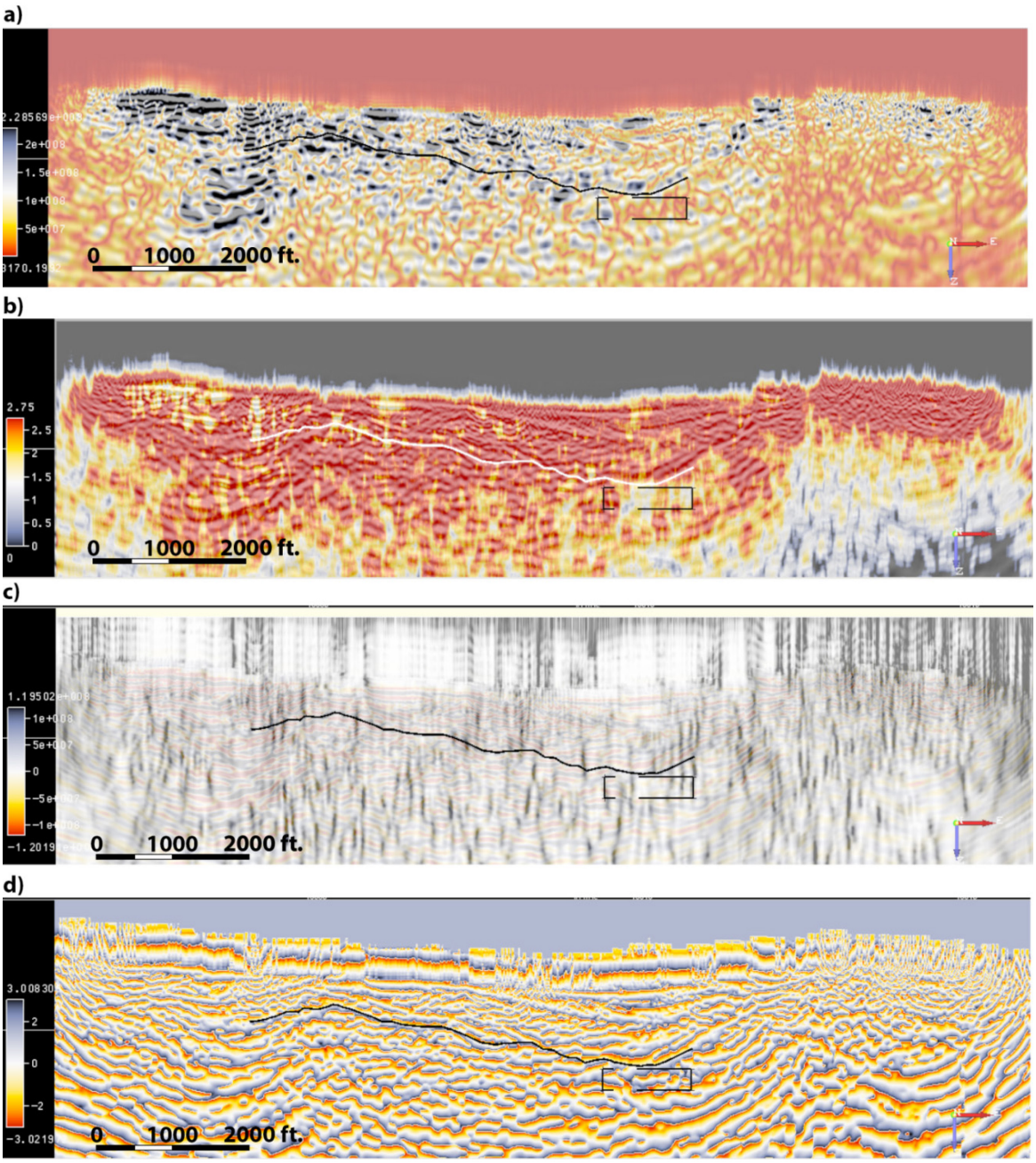

Figure 17- Instantaneous amplitude (a), GLCM entropy (b), similarity (c) and instantaneous phase (d). Thin black lines mark the bottom of the Tertiary section, and a black box marks the ore zone.

3.3 Structural Interpretation

Two structural models are presented in Figure 18. Note that other geologically viable models for Line 3 could exist. There is not a single, unique structural and geometric solution associated with most geologic data. Rather, multiple models can describe the same data.

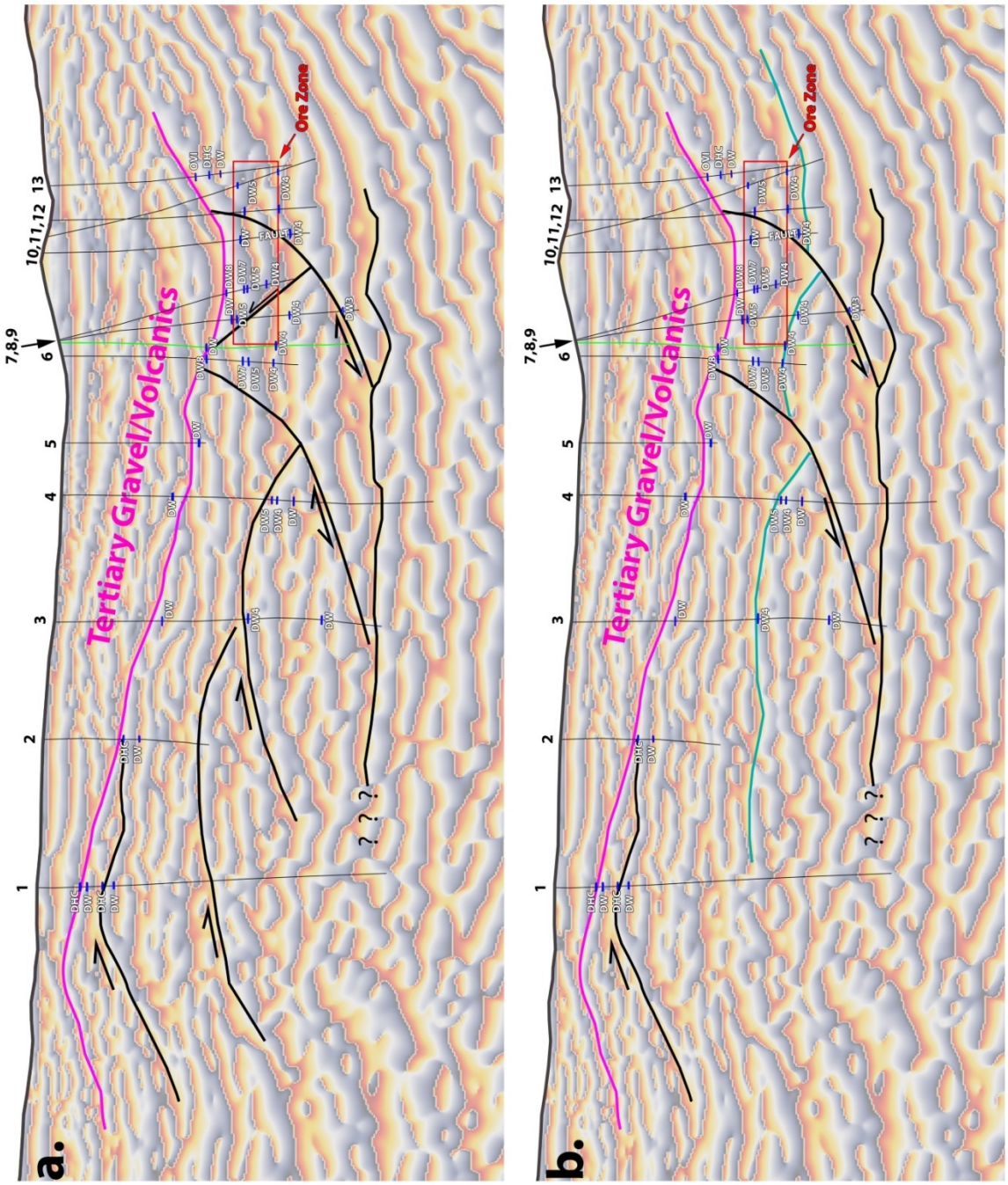

Figure 18 – Two possible structural models with numbered drill holes. A pink line marks the bottom of the Tertiary section, and a thin red box marks the ore zone.

3.4 VSP data

Velocity data were averaged in a similar manner to the petrophysical samples discussed in section 4.2 with the exception of Dw units. The VSP hole was drilled by reverse circulation (RC); RC chips make it difficult to identify specific Wenban units and only Dw4 could be identified. However, Dw units were interpolated to the VSP hole from a nearby core hole, which was about 125 ft to the west of the VSP hole. The results of the velocity averages for given Dw units are shown in Table 5 along with density, which was estimated from P-wave velocity by Gardner's law. Note the 3,705 m/s velocity for Dw Decarbonatized (Dw DECAL).The VSP hole shows a Vp/Vs ratio of 1.8 to 2.2 for the decarbonatized zone. A crossplot of Vp and Vs for the VSP hole is shown in Figure 19; the area highlighted by the red box in the crossplot represents Vp/Vs values that occur in the ore-zone.

	# samples	P-vel (m/s)	std (P-vel, m/s)	S-vel (m/s)	std (S-vel, m/s)	density* (g/cc)	Vp/Vs	Acoustic Imped. Z
TQA	377	2581	1785	859	544	2.21	3.00	5697
Dw8	60	3569	382	1637	116	2.39	2.18	8546
Dw DECAL	65	3705	222	1848	68	2.42	2.00	8959
Dw5	34	5302	378	2103	115	2.64	2.52	14019
Dw4	160	4690	1161	2543	354	2.56	1.84	12016

Table 5- Averages from VSP hole with interpolated lithology logs from near-by core hole.

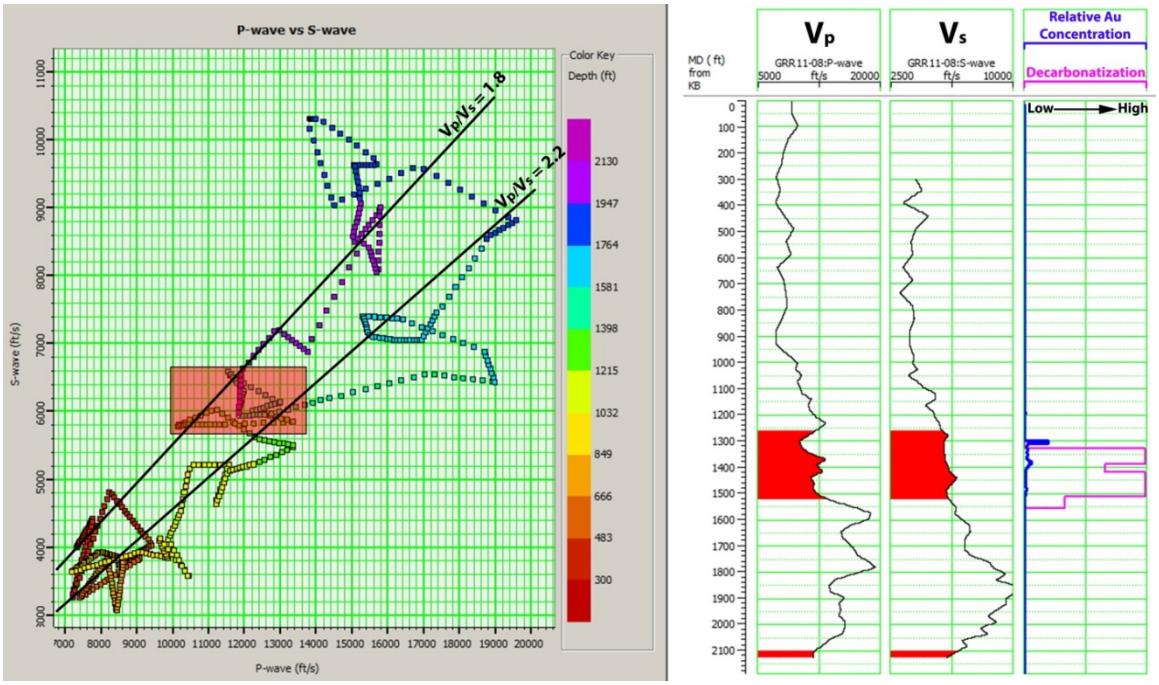

Figure 19 – Crossplot of Vp and Vs down the VSP hole.

4 Discussion

This section is focused on the merits of attribute analysis applied to CTD seismic exploration. Much of this discussion relates back to data quality and determining the feasibility of deriving meaning from attributes calculated in the low S/N data. It is important to learn from previous hardrock studies. However, very little attribute analysis is presented in this relatively new field. Consequently, we must also learn from carbonate oil and gas reservoir analogues.

The discussion begins with the petrophysical data since rock properties are the basis for attribute response.

4.1 Petrophysics

The same petrophysical trends discovered by Smith (2010) within the Cortez Hills area were also observable within the Goldrush setting. However, due to the increased number of samples collected since Smith's work (i.e., 92 samples in the 2010 study compared to 566 samples in this study), I was able to separate unaltered and decarbonatized samples based on a cross-plot of acoustic impedance vs. porosity. The trends do not become entirely apparent until the Wenban unit is segregated from the entire population. The two separate trends may represent primary porosity (i.e., diagenetic) and secondary porosity (i.e., hydrothermal alteration) when looking at the Wenban subset of data (Figure 15). This is logical since decarbonatization is thought to increase porosity in CTD (Hofstra & Cline, 2000; Cline et al., 2005), which is generally known to reduce seismic parameters in carbonate rock (Hart et al., 2004). The separation between the primary and secondary porosity trends is significant, especially when considering that the most strongly altered rock is not competent enough to sample in the petrophysics laboratory. Accordingly, Figure 15 represents a minimum separation between background/unaltered Wenban and altered Wenban.

P-wave velocity from the VSP hole may help validate the hypothesis that there is a severe sampling bias regarding decarbonatized rock; the average P-wave velocity of 3,705 m/s for decarbonatized rock is only 25 m/s less than the 3,730 m/s average calculated from core samples. However, the standard deviation is over 800 m/s. This could indicate that the cross-plot, which was constructed from sampling of core,

represents a minimum separation between unaltered and decarbonatized rock. However, more wire-line velocity data are required to determine a truly representative velocity for strong decarbonatization within the Goldrush deposit.

Figure 20 shows a modified cross-plot of Figure 18, which uses density and porosity measurements from drill-core petrophysics but a constant velocity of 3,705 m/s. This theoretical cross-plot may show a more realistic separation of trends by using the more reliable VSP velocity average for decarbonatization. We would also expect density values to show a similar bias to P-velocities, which would further lower acoustic impedance in this cross-plot. Wire-line density logging is the only tool that would allow for the verification of this bias in drill-core derived densities.

Based on the VSP averages (using Gardner density estimates), the decarbonatization-to-unaltered-Dw5 contact exhibits an acoustic impedance contrast of 22% whereas drill-core measurements produced a contrast of 1.4%. This extreme difference may be due to the sampling bias as previously discussed. Salisbury et al. (2003) state that a 6% acoustic impedance contrast results in a minimum value for strong reflections. Anomalously strong reflections are observable at this contact in the PSDM. However, acoustic impedance inversion would have to be undertaken, to estimate contrasts from the PSDM.

The two petrophysical datasets used in this study (i.e., drill core and VSP) provide contrasting averages for Wenban units. In all cases, the drill-core dataset

underestimated P-velocity relative to the VSP data. The most severe underestimate is for Dw5 (5302 vs. 4162 m/s) and DW4 (4690 vs. 4027 m/s). Acoustic impedance contrasts calculated from the drill-core seismic response database are very low for unaltered, and altered/unaltered contacts of the Wenban Formation (on the order of 1%, see

Table 4). One reason for such differences may be anisotropic effects, which produce yet another form of sampling bias in the drill-core measurements. Strong bedding produces fracturing at layer boundaries that prevents drill-core measurements in the laboratory within certain DW intervals. Energy recorded from the VSP survey is not completely zero-offset; energy therefore may have traveled parallel to the strong bedding and thus increased velocities relative to the ultrasonic laboratory measurements (Larner & Cohen, 1993).

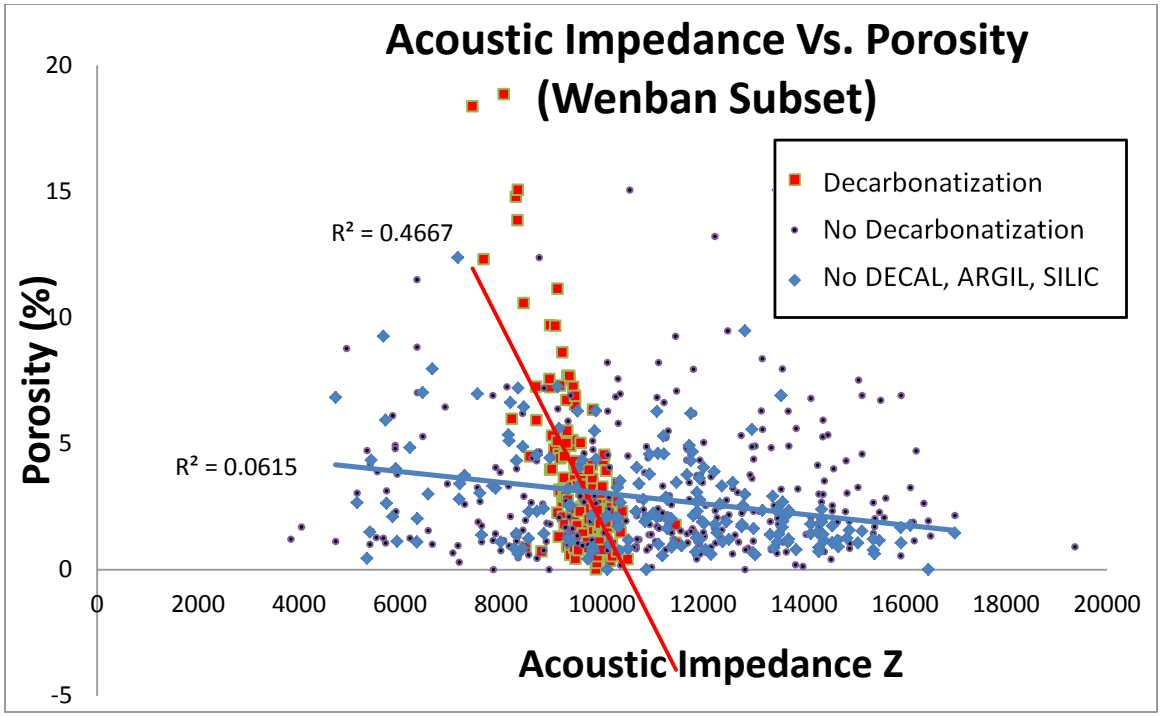

Figure 20 – Porosity vs. theoretical acoustic impedance. Theoretical acoustic impedance was calculated with density values from decarbonatized core samples and a 3,705 m/s velocity from the VSP average.

4.2 Attribute Response

The majority of the ore-zone is characterized by chaotic reflections that exhibit reduced amplitudes and moderate to low frequencies. This zone is encased by higher amplitude reflections, which exhibit a greater degree of continuity. Reduction in amplitude is apparent in the energy and instantaneous amplitude attributes (see Figure 16a and 17a, respectively). Similar seismic characteristics exist towards the margins of the dataset, especially to the east, under the basalt. However, these zones are clearly representative of reduction in data quality and are not related to actual geologic features at depth. Overlying, seismically attenuating basalt produces noise that resembles the seismic

response of the brecciated ore-zone. The ore-zone is surrounded, in both the vertical and lateral direction, by strong reflectors that appear relatively flat in pre-stack gathers. Conversely, zones toward the margins of the dataset, and especially to the east under the basalt, exhibit discontinuous pre-stack events that never grade back into competent reflections. These facts lead us to believe that the chaotic nature of reflections in the ore zone are representative of actual rock-properties, rather than seismic noise.

Smith (2010) found that the modeled ore-zone in the Gold-Acres setting produced a bright spot. The Goldrush PSDM holds true to these observations. However, the thickest ore body modeled by Smith (2010) is 66 ft, which produces constructive interference from the unaltered to altered contacts above and below the ore zone. Accordingly, the modeled ore body appears as one large bright spot. Given the thickness of the Goldrush ore body (~300 ft), tuning effects are not an issue. Accordingly, the tops and bottoms produce individual responses (i.e., subtle bright spots) with a broad dim spot in-between. The bottom contact is most obvious; VSP velocities suggest that this phenomenon is due to greater rock property contrasts at the lower contact. In addition to simple acoustic impedance contrasts, factors such as fracture orientation, pore dimensions and anisotropy have a great effect on amplitude; these are still not well understood within the Goldrush setting. More down-hole logging is required to understand these factors (Wang, 2001).

Studies performed by Sagan and Hart (2006) and Tedesco (1994) indicate that the reduction in amplitude values within the Goldrush ore-zone is similar to that of

carbonate breccias found within the Appalachian Basin, USA. The geologic processes that form hydrothermal dolomite reservoirs (i.e., leaching and dolomitization of limestone by low temperature basinal brine) produce brecciation and sulfidation but the alteration within the Appalachian basin is not as intense as CTD. Furthermore, there is no orogenic overprint. However, since the stratigraphy of the referenced studies in the eastern USA is similar to that of the Goldrush area (in terms of amplitude contrasts above and below brecciation), we gain confidence in this analogue.

The carbonate-hosted Kombat and Tsumeb base-metal deposits of Namibia represent the closest CTD analogue that has been seismically imaged within the mining industry. But, only one seismic image is presented and no attributes were calculated (Stevenson et al., 2003). Furthermore, amplitude dimming of karsted horizons is not discussed. This may be a result of inadequate processing; prospective ground in this area was imaged via the simpler and more approximate process of NMO correction and post-stack migration. Pre-stack depth migration and amplitude preservation performed on the seismic data used in this study is a more robust seismic processing tool that may have allowed for better imaging of mineralization.

Amplitude dimming of events through the brecciated ore-zone is also consistent with siliciclastic gas chimney responses (Arnsten et al., 2007; Meldahl et al., 2001). However, the seismic response is often high in frequency with chaotic features that are far more vertically oriented when compared to the ore-zone. The geologic processes that produce gas chimneys, which are not well understood, may involve interconnected

fracture networks and/or diffusion in sediments (Arnsten et al., 2007). This makes the gas chimney a subordinate analogue relative to hydrothermal dolomite reservoirs (e.g., Appalachian Basin, USA).

Frequency shadows are prevalent under the basalt to the east, which is consistent with observations of wave propagation through volcanic rocks of the Snake River Plain (Pujol & Smithson, 1991). These areas are highlighted by the frequency shadow attribute in Figure 16d. Most research on frequency washout relates to low-frequency shadows below gas charged sediments, which also attenuate the propagating wave (Ebrom, 2004). Such shadows exist within the ore-zone, and may be related to anomalous high-frequency attenuation within the Tertiary units above the ore-zone (note the low frequencies above the ore-zone in Figure 16a). Alternatively, the low frequency response could be related to attenuation within the breccia zone itself, which would have exploration implications.

The sweetness high observed within the ore-zone in Figure 16c is a function of high frequency to energy ratios. There is no literature related to the sweetness attribute as applied to carbonate environments. However, it appears that lower wavelength and lower energy produce sweetness highs within our PSDM dataset; once again, this represents a seismic signature consistent with both the ore zone and the noisy margins of the dataset.

Low GLCM entropy values seen in Figure 17b indicate that the majority of the ore-zone is expressed as a relatively homogenous area. This is counterintuitive and contradicts observations made by Yengu et al. (2010) that suggest high entropy values for altered limestone in Alberta, Canada. The entropy attribute may not provide diagnostic results since the majority of our PSDM section dataset exhibits high disorderliness.

The similarity attribute has successfully defined faulting within altered carbonates of the eastern USA (e.g., the Trenton-Black River reservoir in eastern Ohio; Sagan & Hart, 2006; Hart, 2004). In our case, time and dip-related attributes (e.g., the similarity attribute seen in Figure 17c) were unable to identify structural features. This is due to the wormy and discontinuous character of most of our reflectors. High dissimilarity and dip based variance values predominantly highlighted noise, especially in the vertical direction. The ultimate reason for such noise is most likely due to common reflection point smearing during migration, an inherent problem related to hard-rock seismic data when velocity models do not appropriately represent lateral variations. Figure 17c shows the instantaneous phase attribute, which provides the best visualization of the seismic data for the purposes of structural interpretation. This attribute allows for the delineation of large antiformal shapes within the data that are possible imbricate stacks.

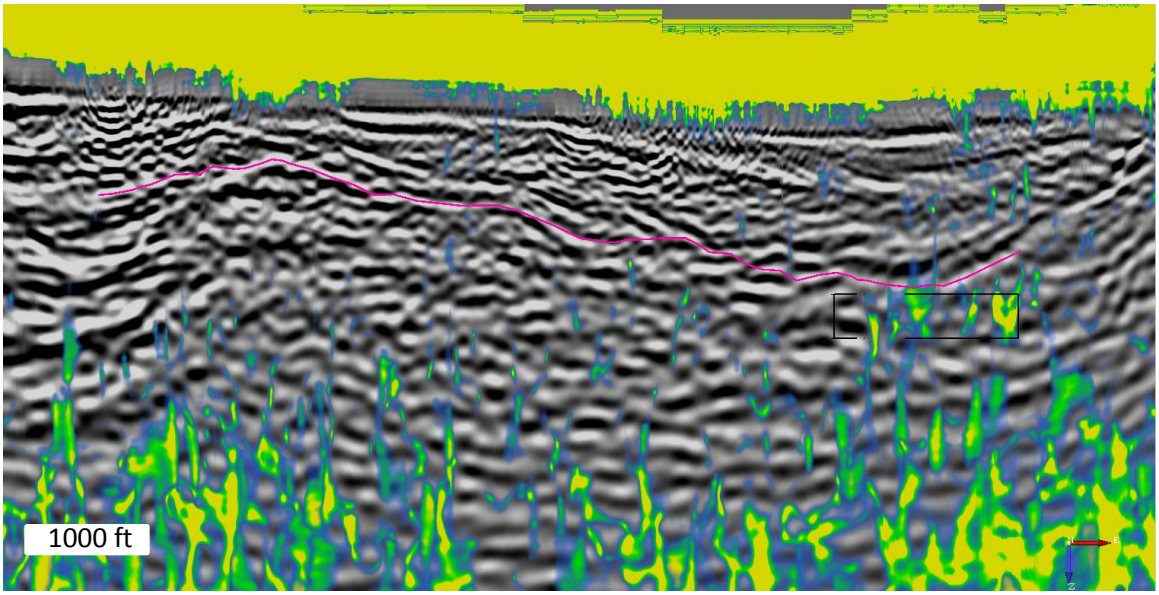

Figure 21 – Sweetness and frequency shadow attributes with modified color bars to highlight the ore-zone. Only the area of high seismic data-quality is shown (migration artifacts towards the margin of the dataset and basalts to the east are subset out of the view). A thin pink line marks the bottom of the Tertiary section, and a black box marks the ore zone. There is no vertical exaggeration.

4.3 Structural Model

The instantaneous phase attribute, shown in Figure 18, transformed the raw amplitude data into a section with sharp and equalized events that allow for improved structural interpretability. This attribute was particularly useful for picking of curved events indicative of possible thrust surfaces.

The imbricate thrust stacks shown in Figure 18a are an interpretation of seismic data alone. Geologic logging indicates undifferentiated DW throughout the proposed roof thrust (drill hole numbers: 1, 2, 3, 4, and 5), which makes this duplex structure model highly speculative. However, the arcuate reflectors, which are visible in the original PSDM and highlighted by the instantaneous phase attribute, suggest the presence of

stacked thrust sheets. Additionally, logging of drillholes near Line 4 to the north, suggest that the model proposed in Figure 18 is feasible. Here, a DW4 over DW5 contact exists at an arcuate reflector. Furthermore, an antiformal structure of similar wavelength and size is imaged in all four seismic lines; the axis of this possible fold structure exhibits a trend similar to that of the ore body (i.e., N30°W).

The pair of listric faults shown in Figure 18a may explain the presence of curved reflectors within the eastern portion of the seismic section. Here, reflectors may represent rollover in the hanging wall of listric normal faults. One interpretation for these listric faults could include normal faulting that reactivated older thrust surfaces, which is documented in the Sevier fold-thrust belt in Utah, Idaho, and Wyoming (Constenius, 1996). Normal movement could have conceivably occurred during Tertiary extension but must predate the overlying Eocene volcanics, since no displacement of reflectors is observed in the Tertiary fill. Geologic logging in drill hole number 10 indicates a substantial amount of faulting (101 continuous ft) that supports the interpretation of the easternmost listric fault. The backthrust shown in Figure18a is supported by thickening of DW5 in drill hole number 8 as well as discontinuous reflections in this area.

Figure 20b introduces an alternative, simpler structural model. Here, thrusting is only illustrated where confirmed by drilling (i.e., DHC repetition in the northwestern portion of the seismic section). The normal listric faults shown in this interpretation could be explained in the same manner as mentioned in the previous paragraph. Furthermore,

they could plausibly sole into an extensional detachment fault, which could be represented as the floor thrust in Figure 20b (Constenius, 1996). This model, however, may not be likely due to the widespread occurrence of older-over-younger DW relationships in the Goldrush area.

The decollement horizon for thrusting or normal slip is represented as a strong, sub-horizontal reflector in Figure 18a. This pick is speculative due to a lack of core drilling and degraded seismic quality at this depth. It may exist deeper in the section.

5 Conclusions

Both carbonate petroleum and CTD exploration attempt to better understand diagenetic environments and overprinting geologic processes that increase porosity and permeability of the carbonate host rock (Cook & Corboy, 2004). Much of the literature pertaining to seismic attribute analysis in the carbonate environment aims at defining stratigraphic and morphological features of the passive-margin platform-slope setting. In most oil and gas reservoirs, this setting exhibits little structural deformation, which produces high signal-to-noise seismic data amenable to a broad spectrum of attribute analysis. In CTD seismic, time-based attributes, such as coherency, dip and derivatives thereof, cannot accurately define diagenetic due to the discontinuous and wormy nature of reflections. Tertiary tuffs and basalts produce multiples and degrade seismic quality. The orogenic and magmatic overprint on the carbonate platform-slope setting of northeast Nevada make interpretation of attributes more difficult. However, this

study has shown that CTD alteration may produce a chaotic dim-spot in PSDM data, which can be highlighted via seismic attribute analysis. Furthermore, smoothed instantaneous phase provides enhanced visualization of reflectors for structural interpretation.

The vast majority of hard-rock seismic mineral exploration studies performed in the past have not had the advantage of imaging stratigraphic features such as porous breccia zones. The porosity and associated fluid/water content of carbonate breccias in the CTD environment allow for a more robust approach to seismic analysis when compared to these previous studies. Increased zones of porosity produce significant rock property contrasts between altered and unaltered limestone in the Goldrush environment. In the case of Line 3, simple observation of reflection coefficients within the PSDM was sufficient to observe the dim-spot, which is coincident with these zones of increased porosity. Furthermore, analogues, such as the Trenton-Black River carbonates of the Appalachian Basin, suggest that the chaotic dim-spot associated with the Goldrush breccia is a defining seismic characteristic of alteration in this area.

The sweetness and frequency washout attributes best highlight the ore. Isolated pockets of increased frequency washout and sweetness may be indicative of alteration, whereas broad zones represent seismic noise and attenuation of signal not related to the ore-zone. These attributes are capable of highlighting seismically attenuating areas having chaotic reflections, which may be indicative of brecciation and alteration. However, both of the responses are highly variable within the ore-zone and should

therefore be used with caution. Smoothing via lateral median filtering proved to be an important tool in improving the interpretability of CTD seismic data for structure, particularly when the smoothed PSDM was used as an input for instantaneous phase calculation.

More advanced studies are warranted, such as seismic inversion and well-property prediction via neural networks. These studies require a shift towards the oil and gas industry approach, which involves defining stratigraphy by downhole geophysical logging. In this study, drill-core petrophysics proved to be a very important tool in establishing trends between unaltered and altered rock. With enough samples, a statistically significant relationship between alteration and petrophysical properties can be ascertained. However, the accuracy and resolution of core data does not appear to be sufficient to replicate wire-line logs for the purposes of advanced processing such as forward modeling, well-property prediction or inversion. Ideally, three to five sonic or VSP logs in addition to one density log per 2D line would allow for appropriate control for both rock-property prediction and seismic-to-well ties. One density log would allow for a modification of coefficients in Gardner's equation to better suit the CTD environment. This would provide fairly accurate estimates of density from all sonic or VSP holes and a better chance at porosity prediction via neural network analysis.

6 References

Adam, E. et al., 2003. 3D imaging for VSM deposit exploration, Matagami, Quebec, *in* D. Eaton, B. Milereit and M. Salisbury, eds. Hardrock Seismic Exploration: Society of Exploration Geophysicists Geophysical Development Series 10, 229-245.

Arnsten, B., Wensaas, L., Loseth, H. and Hermanrud, C., 2007. Seismic modeling of gas chimneys. Geophysics, **72**, no. 5, SM251-SM259.

Bellefleur, G., Malehmir, A. and Muller, C., 2012, Elastic finite-difference modeling of volcanic-hosted massive sulfide deposits: A case study from Half Mile Lake, New Brusnwick: Geophysics, **77**, no. 5, WC25-WC36.

Boni, M., Terracciano, R., Evans, N.J., Laukamp, C., Schneider, J. and Bechstadt, T., 2007, Genesis of Vanadium ores in the Otavi Mountainland, Namibia: Economic Geology, **102**, 441-569.

Boyer, S.E. and Elliot, D., 1982, Thrust systems: AAPG Bulletin, **66**, 1196-1230.

Brown, A., 2012, Dim spots: opportunity for future hydrocarbon discoveries?: The Leading Edge, **31**, 682-683.

Brown, A. R., 2001, Understanding seismic attributes: Geophysics, **66**, 47-48.

Brown, A. R., 2011. Interpretation of three-dimensional seismic data, 7 ed.: American Association of Petroleum Geologists.

Castagna, J., Swan, H. and Foster, D., 1998, Framework for AVO gradient and intercept interpretation: Geophysics, **53**, 948-956.

Chopra, S. and Alexeev, V., 2005, Application of texture attribute analysis to 3D seismic data: CSEG Recorder, **30**, 29-32.

Chopra, S. and Marfurt, J. K., 2005, Seismic attributes - a historical perspective: Geophysics, **70**, no. 5, 3SO-28SO

Chopra, S. and Marfurt, J. K., 2007, Seismic attributes for fault/fracture characterization: SEG Technical Program Expanded Abstracts, 1520-1524.

Chopra, S. and Marfurt, J. K., 2007, Seismic attributes for prospect identification and reservoir characterization: Society of Exploration Geophysicists, Geophysical Developments no. 11.

Cline, J. S., Hofstra, A.H., Muntean, J.L., Tosdal, R.M., and Hickey, K.A., 2005, Carlin-Type Gold Deposits in Nevada: Critical Geologic Characteristics and Viable Models: Economic Geology, **100**, 451-483.

Constenius, K.N., 1996, Late Paleogene extensional collapse of the Cordillera foreland fold and thrust belt: Geological Society of America Bulletin, **108**, 20-39

Cook, H. and Corboy, J., 2004, Great Basin Paleozoic carbonate platform: facies, facies transitions, depositional models, platform architecture, sequence stratigraphy, and predictive mineral host models: U.S. Geological Survey Open-File Report 2004-1078 Field Trip Guidebook—Metallogeny of the Great Basin Project, August 17—22, 2003.

DeCelles, P., Gehrels, G., Quade, B. and LeReau, B., 2004, Late Jurassic to Eocene evolution of the Cordilleran thrust belt and foreland basin system, western USA: American Journal of Science, **304**(2), 105-168.

Dehgannejad, M., Malehmir, A., Juhlin, C. and Skytta, P., 2012, 3D constraints and finite-difference modeling of massive sulfide deposits: The Kristineberg seismic lines revisited, northern Sweden: Geophysics, **77**, no. 5, WC69-CW79.

Duff, D., Hurich, C. and Deemer, S., 2012, Seismic properties of the Voissy's Bay massive sulfide deposit: insights into approaches to seismic imaging: Geophysics, **77**, no. 5, WC59-WC68.

Eaton, D., Milkereit, B. and Salisury, M., 2003, Hardrock Seismic Exploration: Mature Technologies Adapted to New Exploration Targets. *In* D. Eaton, B. Milkereit and M. Salisury, eds., Hardrock seismic exploration: Society of Exploration Geophysicists Geophysical Development Series 10, 1-6.

Ebrom, D., 2004, The low-frequency gas shadow on seismic sections: The Leading Edge, **23**, 772.

Evans, B., Urosevic, M. and Taube, A., 2003, Using surface-seismic reflection to profile a massive sulfide deposit at Mount Morgan, Australia. *In* D. Eaton, B. Milkereit and M. Salisbury, eds., Hardrock Seismic Exploration: Society of Exploration Geologists Geophysical Development Series 10, 157-163.

Gardner, G., Gardner, L. and Gregory, A., 1974, Formation velocity and density - the diagnostic basic for stratigraphic traps: Geophysics, **39**, 770-780.

Gibson, M., 2011, Application of seismic to mineral deposit exploration and evaluation: The Leading Edge, **60**, 616-620.

Hampson, D. P., Scheulke, J. S. and Quirein, J. A., 2001, Use of multiattribute transforms to predict log properties from seismic data: Geophysics, **66**, 220.

Han, D., Nur, A. and Morgan, D., 1986, Effects of porosity and clay content on wave velocities in sandstones: Geophysics, **51**, 2093-2107.

Harrison, C. B. and Urosevic, M., 2012, Seismic processing, inversion, and AVO for gold exploration - case study from Western Australia: Geophysics, **77,** no. 5, 235-243.

Hart, B., Atroshi, K., Sagan, J. and Tebo, J., 2004, Seismic Imaging of diagenesis: a tool for studying hydrothermal dolomite systems: 43rd Annual Conference, Ontario Petroleum Institute No. 3.

Heinonen, S, Imana, M., Snyder, D., Kukkonen, I., Heikkinen, P., 2012, Seismic reflection profiling of the Pyhasalmi VHMS-deposit: a complementary approach to the deep base metal exploration in Finland: Geophysics, **77**, no. 5, WC15-WC23.

Hofstra, A. and Cline, J., 2000, Characteristics and models for Carlin-type gold deposits: Reviews in Economic Geology, **13**, 163-220.

Jackson, M., Arbonies, D. and Creel, D., 2010, Architecture of the Cortez Hills Breccia Body: Geological Society of Nevada Great Basin Evolution and Metallogeny, 97-123.

John, D., Christopher, H. and Colgan, J., 2008, Magmatic and tectonic evolution of the Caetano caldera, north-central Nevada: A tilted, mid-Tertiary eruptive center and source of the Caetano Tuff: Geosphere, **4**, 75-106.

Larner, K. and Cohen, J., 1993, Migration error in transversely isotropic media with linear velocity variation in depth: Geophysics, **58,** 1454-1467.

Leonardson, R. W., 2010. Barrick Cortez Gold Acres Structure: Geological Society of Nevada Great Basin Evolution and Metallogeny, 17-29.

Liner, C., 2004, Elements of 3D seismology 2nd ed., PennWell.

Loucks, R., Kerans, C., Janson, X. and Rojano, M., 2011, Lithofacies analysis and stratigraphic architecture of a deep-water carbonate debris apron; Lower Cretaceous (latest Aptian to latest Albian) Tamabra Formation, Poza Rica Field Area, Mexico. *In* R. Shipp, P. Weimer and H. Posamentier, eds., Mass-transport deposits in deepwater settings: Society for Sedimentary Geology, 367-389.

Louie, J. N., Pullammanappalil, S. K. and Honjas, W., 2011, Advanced imaging for geothermal development: Proceedings of the New Zealand Geothermal Workshop.

Louie, J., Pullammanappallil, S. and Honjas, W., 2012, Advanced seismic imaging for geothermal development: expanded abstract, Society of Exploration Geophysicists 82nd Annual Meeting, Las Vegas, http://dx.doi.org/10.1190/segam2012-0965.1, 6 pp.

MacKay, S., 2011, The interpreter's guide to depth imaging. SEG San Antonio 2011 Annual Meeting, 975-979.

Meldahl, P., Heggland, R., Bril, B. and Groot, P. d., 2001, Identifying faults and gas chimneys using multiattributes and neural networks: The Leading Edge, **20**, 474-482.

Muntean, J. and Taufen, P., 2011, Geochemical exploration for gold through transported alluvial cover in Nevada: examples from the Cortez Mine: Economic Geology, **106**, 806-833.

Muntean, J., Cline, J., Simon, A. and Long, A., 2011, Magmatic-hydrothermal origin of Nevada's Carlin-type gold deposits: Nature Geoscience, **14**, 122-127.

Muntean, J., Coward, M. and Tarnocai, C., 2007, Reactivated Paleozoic normal faults: controls on the formation of Carlin-type gold deposits in north-central Nevada. *In* R. Butler and R. Graham, eds., Deformation of the Continental Crust – The Legacy of Mike Coward: Geological Society Special Publication, 573-589.

Nutt, C. J., 2005. Role of low-angle to bedding-parallel faults in localizing Carlin-type gold, Northern Nevada. Geological Society of America Annual Meeting Abstracts with Programs, 418.

Ponce, D. and Glen, J., 2008, A prominent geophysical feature along the northern Nevada rift and its geologic implications, north-central Nevada: Geosphere, **4**, 207-217.

Pujol, J. and Smithson, S., 1991, Seismic wave attenuation in volcanic rocks from VSP experiments: Geophysics, **9**, 1441-1455.

Sagan, J.A., Hart, B.S., 2006, Three-dimensional seismic-based definition of fault-related porosity development: Trenton-Black River interval, Saybrook, Ohio: AAPG Bulletin, **90**, 1763-1785.

Sams, M., Neep, J.., Worthington, M., and King, M., 1997, The measurement of velocity dispersion and frequency-dependent intrinsic attenuation in sedimentary rocks: Geophysics, **62**, 1456-1464

Smith, J. B., 2010, Seismic Reflection as a Direct Detector of Gold Mineralization in the Carlin District, USA: Honours Thesis, Curtin University.

Smith, M., Dickinson, W. and Gehrels, G., 1993, Contractional nature of Devonian-Mississippian Antler tectonism along the North American continental margin Geology, **21**, 21-24.

Stevenson, F., Higgs, R. and Durrheim, R., 2003, Seismic Imaging of Precious and Base-Metal Deposits in Southern Africa, *In* D. Eaton, B. Milkereit and M. Salisbury, eds., Society of Exploration Geophysicists Hardrock Seismic Exploration, Geophysical Development Series 10, 141.

Tanner, M. T., Koehler, F. and Sheriff, R. E., 1979, Complex trace analysis: Geophysics, **44**, 1041-1063.

Tedesco, S., 1994, Integrated exploration locates Cincinnati arch dolomite breccias: Oil and Gas Journal, 86.

Telford, W. M., 1990, Applied Geophysics, 2nd ed.: Cambridge University Press.

Townsend, J., Sampson, L. and Bourne, B., 2010, Recent advances in the application of geophysics for gold exploration in the north-central Great Basin: Geological Society of Nevada Great Basin Evolution and Metallogeny, 167-177.

Tsvankin, I. and Thomsen, L., 1994, Nonhyperbolic reflection moveout in anisotropic media: Geophysics, **59**, 1290-1304.

Urosevic, M. and Kepic, A., 2008, Hard rock seismic exploration of ore deposits in Australia: SEG Annual Meeting Program, 3613.

Wang, Z., 2001, Fundamentals of seismic rock physics: Geophysics, **66**, 398-410.

West, B. P., May, S. R., Eastwood, J. and Rossen, C., 2002, Interactive seismic facies classification using textural attributes and neural networks: The Leading Edge, **21**, 1042-1049.

White, D. and Malinowski, M., 2012. Interpretation of 2D seismic profiles in complex geological terrains: Examples from the Flin Flon mining camp, Canada: Geophysics, **77,** no. 5, WC37-WC46.

Yengu, M., Kurt, M. and Matson, S., 2010, Seismic texture analysis for reservoir prediction and characterization: The Leading Edge, **29**, 1116-1121.

Yushun, D., Zhaoquan, P., Lingbang, Z. and Mingbo, B., 2011, Carbonate reservoir and gas-bearing property detection using sweetness: SEG Annual Meeting, 1197-1201.